Journal of
Bioinformatics and Comparative Genomics

JScholar
Fostering Scholarly Communication

Research Article Open Access

In Silico Discovery of Potential Japanese Encephalitis Antagonists Targeting the NS5 RNA-Dependent RNA-Polymerase

Aishwarya Mahadevan, Nirmitee Mulgaonkar, Haoqi Wang, and Sandun Fernando*

Biological and Agricultural Engineering Department, Texas A&M University, United States

***Corresponding author:** Sandun Fernando, Biological and Agricultural Engineering Department, Texas A&M University, United States, Tel: +19795719958. E-mail: sfernando@tamu.edu

Received Date: April 20, 2021 **Accepted Date:** May 20, 2021 **Published Date:** May 22, 2021

Citation: Aishwarya Mahadevan (2021) *In Silico* Discovery of Potential Japanese Encephalitis Antagonists Targeting the NS5 RNA-Dependent RNA-Polymerase. J Bioinfo Comp Genom 4: 1-25

Abstract

Japanese encephalitis (JE) is a flaviviral brain infection threatening large populations in different parts of the world, caused by an arbovirus Japanese encephalitis virus (JEV). Apart from severe symptoms, the disease carries an alarming death rate of about 30%. Although vaccination is available as a preventive measure, there are no drugs to treat the disease once contracted. This study reports four molecules that can serve as lead compounds screened via molecular docking and molecular dynamics simulations targeting the RNA-dependent RNA polymerase (RdRp) domain of the nonstructural protein 5 (NS5) of JEV. The four lead compounds are ZINC9972155, ZINC67912950, ZINC95910070, and ZINC196939367 from the ZINC database. The lead compounds have significantly higher affinities to the RdRp domain of JEV NS5 than the native nucleotides indicating that they have the potential to serve as effective competitive inhibitors.

Keywords: Japanese encephalitis virus; inhibitors; RNA-dependent RNA-polymerase; NS5

Introduction

Japanese encephalitis (JE) is a flaviviral brain infection caused by an arbovirus, the Japanese encephalitis virus (JEV). Anthropophilic mosquitoes of the *Culex* species (mainly the *Culex tritaeniorhynchus* group) that breed in rice fields are mainly known to transmit JEV. JEV was first reported in Japan in the 1870s. It spread to the south, east, and south-east of Asia and now to the Western Pacific, threatening large populations [1-3]. It can cause severe viral-encephalitis in 0.1–2% of people infected, with a death rate of 20–30%, and of those that survive, suffer from severe neurologic injuries, including persistent motor defects and severe cognitive and language impairments. Acute encephalitis develops in about 0.1–2% of cases, producing serious neurological lesions in 30-50% of the survivors [2-6].

Infections with JEV most often produce no symptoms (asymptomatic), which is why only 0.3% of cases produce clinical features. The first signs of disease appear after an incubation period of between 6 and 14 days, usually begins with a high fever, chills, muscle pain, and meningitis-type headaches accompanied by vomiting. The initial clinical features in children usually involve gastrointestinal symptoms (nausea, vomiting, and abdominal pains). These nonspecific symptoms can continue for 2–4 days. After this period, the patient's condition declines rapidly. About 85% of the infected suffer from seizures. The meningeal syndrome prevails, causing painful neck stiffness. Additionally, motor paralyzes, including hemiplegia and tetraplegia, may also occur. In about 30% of patients, tremors, rigidity, abnormal movements, and other signs of extrapyramidal involvement are present. Recovery usually leaves serious behavioral and neurological injuries such as persistently altered sensorium, extrapyramidal syndrome, epileptic seizures, and severe mental retardation in children [7, 8]. Vaccines for the prevention of JEV are available and have reduced the occurrence of JE in some countries. However, they are not effective against all the clinical subjects causing 10,000 – 15,000 human deaths and 709,000 disability-adjusted life years annually. Regardless of the vaccine development, there is a lack of an absolutely protective or preventive vaccine or antiviral drugs to treat JE. Hence, there is an urgent need to identify lead compounds with antiviral properties against JEV [9] so that a drug could be developed.

JEV belongs in the genus *Flavivirus* of the *Flaviviridae* family, which also includes the important human pathogens Zika virus (ZIKV) and the Dengue virus (DENV). Flaviviruses replicate their RNA genome using virally encoded replication proteins. Hindering the flaviviral replication is widely studied and considered to be an effective antiviral drug discovery approach. Recent studies have led to the identification of specific domains in the flaviviral proteins whose inhibition could block viral replication. Antiviral agents for flaviviruses hepatitis C virus, Dengue virus, and West Nile have been reported [10]. Similar inhibitors with antiviral properties for JEV were reported that targets the NS3 - Indirubin, Dehydroepiandrosterone (DHEA), N-nonyl-deoxynojirimycin, and SCH 16 [11]. Nevertheless, only a few JEV inhibitors have been discovered and are undergoing clinical trials at present. It is also important to note that despite the severe consequences of the infection, efforts for drug discovery against JEV have been relatively very limited.

Viruses contain and produce structural, nonstructural proteins, regulatory and accessory proteins for different functions. The nonstructural proteins, coded for by the viral genome, are expressed in infected host cells and not assembled in the virion. These proteins play an important role in the flaviviral RNA genome replication and assembly processes. Specifically, nonstructural proteins NS3 and NS5 are reported as the main components of the viral RNA replication complex associated with the 3′ noncoding region of genomic RNA in the initiation of viral replication. NS5 is the largest and most conserved flavivirus protein encoded in the open reading frame. NS5 harbors two domains that directly affect viral replication - methyltransferase (MTase) in its N-terminal (≈265 residues) responsible for RNA capping (methylation of the 5′ RNA cap structure); and RNA-dependent RNA polymerase (RdRp) within the C-terminal (≈640 residues) for viral replication, and hence was considered a potential drug target in this study [12,13].

The goal of this work was to identify potential antagonists to hinder viral replication via silencing NS5 without causing toxicity to the infected by analyzing the ligand-receptor interactions between the NS5 receptor and the pharmacologically active ligands screened from the ZINC database [14] using a combination of molecular docking and molecular dynamics (MD) simulations. Docking was used to identify the ligand hotspot on the receptor, as well as, to analyze the screened compounds. Molecular dynamics was used for druggability assessment and to further verify binding free energies between the ligand(s) and receptor in a simulated cellular environment while the protein was dynamically flexing.

Computational methods

Protein structure analysis

The crystal structure of JEV NS5 was available in the Protein Data Bank (PDB ID:4K6M) [15, 16]. NS5 performs the main activities pertinent to viral replication with the help of its enzymatic domains – MTase and RdRp. The MTase activity protects viral mRNA from degradation by 5′-exoribonucleases and ensures their recognition by the eukaryotic translation initiation factor. The N-terminal MTase domain (residues 5–266) is connected through a ten-residue linker to the C-terminal RdRp domain formed by residues 276–895. In turn, the RdRp domain is formed by three subdomains called fingers, palm, and thumb. The RdRp domain contains the core polymerase that is essential for the viral RNA synthesis and, thus, is of major interest as a potential drug target. The protein crystal has two chains, A and B, comprising three NS5 hexamers, of which chain A was computationally isolated using VMD [17] for all the studies in this work. The RdRp active site of JEV NS5 protein – chain A was visualized using VMD and used for docking and MD simulations.

NTP interactions with JEV NS5 RdRp

The conserved RdRp domain of JEV NS5 protein was examined using AutoDock Vina [18]. Nucleotide triphosphates (NTPs): adenosine triphosphate (ATP), guanosine triphosphate (GTP), cytidine triphosphate (CTP), and uridine triphosphate (UTP) which are building blocks of nucleic acids were used as ligands. The JEV NS5 (PDB ID:4K6M) crystal structure was retrieved from PDB [16]. The 3D structures of the ligands were obtained from the ZINC15 database [14], ATP (ZINC4261765), GTP (ZINC60094177), CTP (ZINC3861746), and UTP (ZINC3861755). The receptor and ligands were prepared using AutoDock Tools [19] and converted to the PDBQT formats. A grid box of size $104 \times 102 \times 116$ Å^3 located at the RdRp domain was generated for docking. The default docking protocol was used to dock the native ligands at the RdRp active site of JEV NS5 protein via AutoDock Vina, a fast and accurate tool for screening out small molecules that are less effective for target sites.

Druggability Assessment of JEV NS5 protein

Probe-based mixed-solvent MD simulations were performed to explore the binding site of the JEV NS5 protein [20-22]. The NAMD simulation [23] configuration files were built using the VMD plugin DruGUI [24]. Five water-soluble organic probes, 60% isopropanol and 10% each of isobutene, acetamide, acetate, and isopropylamine were used for druggability analyses to reveal any clusters of hotspots that specify the presence of druggable sites on the receptor. Chemistry at HARvard Macromolecular Mechanics (CHARMM) force fields for larger proteins and the CHARMM General Force Fields (CGenFF) for smaller ligands were used for the simulations [25, 26]. The solvent model for MD was TIP3P. The protein was immersed in a 6 Å width water solvent. The protocol of the simulation had three steps, system minimization and equilibration, and unrestrained MD simulation. First, the system was minimized with 1.0 scale of constraints under 0K for 4ps. The equilibration step then typically raised the system temperature from 100K to 600K, eventually stabilizing at 300K. The whole equilibration step took 1.4ns to complete. Finally, unconstrained MD simulations were carried out for 40ns at 1.01325atm and 300K under isothermal-isobaric (NPT) conditions. The simulation output files were analyzed by the standard protocol described in the plugin documentation for all the probe molecules [24]. All probe molecules were shown with binding free energies (druggability score) given and ranked, with some of the probe molecules grouped into different clusters. These active probe molecules were considered as potential pharmacophores based on their functional groups and probe-protein interactions.

Pharmacophore Identification

Enhanced Ligand Exploration and Interaction Recognition Algorithm (ELIXIR-A) [27-30] (ELIXIR-A) was used for deciphering pharmacophores via protein-ligand interactions analyses done using the NAMD and molecular docking studies. ELIXIR-A is a pharmacophore screening algorithm that is under development in our laboratory. It consists of a computer-guided routine that recognizes pharmacophore points i.e., the ensemble of steric, electrostatic, and hydrophobic properties which are essential for optimal supramolecular interactions with the receptor to inhibit its biological effect. The probe molecules were converted to pharmacophores using the ELIXIR-A VMD plugin. The pharmacophores with good druggability scores were used for further ligand screening.

Ligand Screening and Verification

Using the pharmacophore information obtained from ELIXIR-A, potential compounds were screened from the ZINC15 database [14] using the ZINCPharmer software [31]. The ZINC15 database includes 122 million conformations for

approximately 13 million molecules. Structure-based screening focuses on matching small molecule conformations with suitable pharmacophores based on the functional groups present at the binding site. The molecules were screened based on their structural stability and having a minimum of three pharmacophore points. The screened molecules were validated *In Silico* via AutoDock Vina using the molecular docking method previously described in the NTP interaction section [32]. Vina evaluated the docking of each small molecule using a scoring function and retained the nine most stable conformations with the best binding score (i.e., the lowest binding affinity). The compound with the highest affinity amongst the screened molecules was selected for MD simulations.

MD simulations

To analyze the conformational and interaction stability of the JEV NS5 protein complexed with ZINC 9367, an MD simulation of 100 ns was performed by using the Schrödinger-Desmond platform [33]. JEV NS5 complexed with ATP was also simulated similarly and was considered as a control. The protein was prepared by Maestro's Protein Preparation Wizard [34, 35]. The missing side chains and loops were added by the Prime module. Ligands were prepared by the LigPrep [36] module that generated 32 stereoisomers per ligand under the OPLS3e force field [37]. These ligands were also ionized using the Epik [38] module at pH 7.0 ± 2.0. AutoDock Vina removed all charge or non-polar hydrogens from the ligands, which were necessary for MD simulations. Here, Schrödinger's Glide [30] XP (extra-precision) module was used to reproduce the docking pose of the complete ligand structure based on the Vina docking results. The reproduced binding pose with the highest glide score (most negative) for each ligand was used as the initial frame for MD. The system was immersed using the TIP3P solvent model under orthorhombic boundary conditions with a buffer distance of 10 Å. The salt concentration of 0.1M was added, and the system charge was neutralized using sodium and chloride ions. Each system was initially minimized under the OPLS3e force field using Desmond's default relax protocol. After relaxation, the systems were simulated under the NPT ensemble at 300 K and 1.01325 bar pressure for 100 ns. Total 500 frames were recorded at an interval of 200 ps excluding the initial frame. Post-simulation analysis included complex root mean square deviations (RMSD), and ligand/protein root mean square fluctuations (RMSF), and complex interactions given by the Simulation Interaction Diagram (SID) module.

Calculation of the binding free energy

The binding free energy of each protein-ligand complex was computed using the Molecular Mechanics/Generalized Born Surface Area (MM/GBSA) method [39]. The python script "thermal_mmgbsa.py" from Schrodinger that utilizes the VSGB 2.0 solvation model with the OPLS3e force field was used to calculate the Prime MM/GBSA free energies [40]. For the entire 100 ns simulation, a total of 500 frames were generated, and 50 frames were sampled uniformly from the entire trajectory for calculation. The free energy of binding (ΔG) for each protein-ligand complex is calculated as follows:

$$\Delta G_{(bind)} = E\_complex_{(minimized)} - (E\_ligand_{(minimized)} + E\_receptor_{(minimized)})$$

Results and discussion

NTP interactions with JEV NS5 RdRp

The docking results showed that the NTPs bind in the same pocket which was previously identified as the active site of the RdRp domain of JEV NS5 protein. The protein-ligand interaction analyses (Figure 1) revealed that THR609, TYR610, SER666, and SER801 were common residues that interacted with the NTPs at the RdRp active site. Table 1 gives the information of the type of bonds formed and the maximum binding affinities of NTPs with the JEV NS5 RdRp domain. Amongst all NTPs, GTP (-7.3 kcal/mol) recorded the highest docking score at the JEV RdRp active site followed by ATP (-6.9 kcal/mol), UTP (-6.6 kcal/mol), and CTP (-6.5 kcal/mol). Small molecules that can bind to the same region with a much higher affinity (i.e., a more negative docking score) could potentially be promising candidates as potent drugs inhibiting the replication cycle of the virus. Hence, the results generated from molecular docking studies were used to filter the pharmacophores which were later used for compound screening.

Table 1: Interaction of NTPs with JEV NS5 RdRp residues

Ligand Name	Interacting residues	Type of bond	H-bond distance (Å)	H-bond donor-acceptor angles	Docking score (kcal/mol)
ATP	LYS459	Hydrogen	2.21	178.94˚	-6.9
	ASP669		1.92	150.76˚	
	SER715		2.16	143.33˚	
GTP	ASP668		2.03	137.82˚	-7.3
	CYS714		2.2	139.85˚	
CTP	SER604		1.98	137.14˚	-6.5
	TYR610		1.97	130.22˚	
	SER666		2.15	125.40˚	
UTP	THR609		2.39	110.0˚	-6.6
	ASN613		2.07	154.47˚	

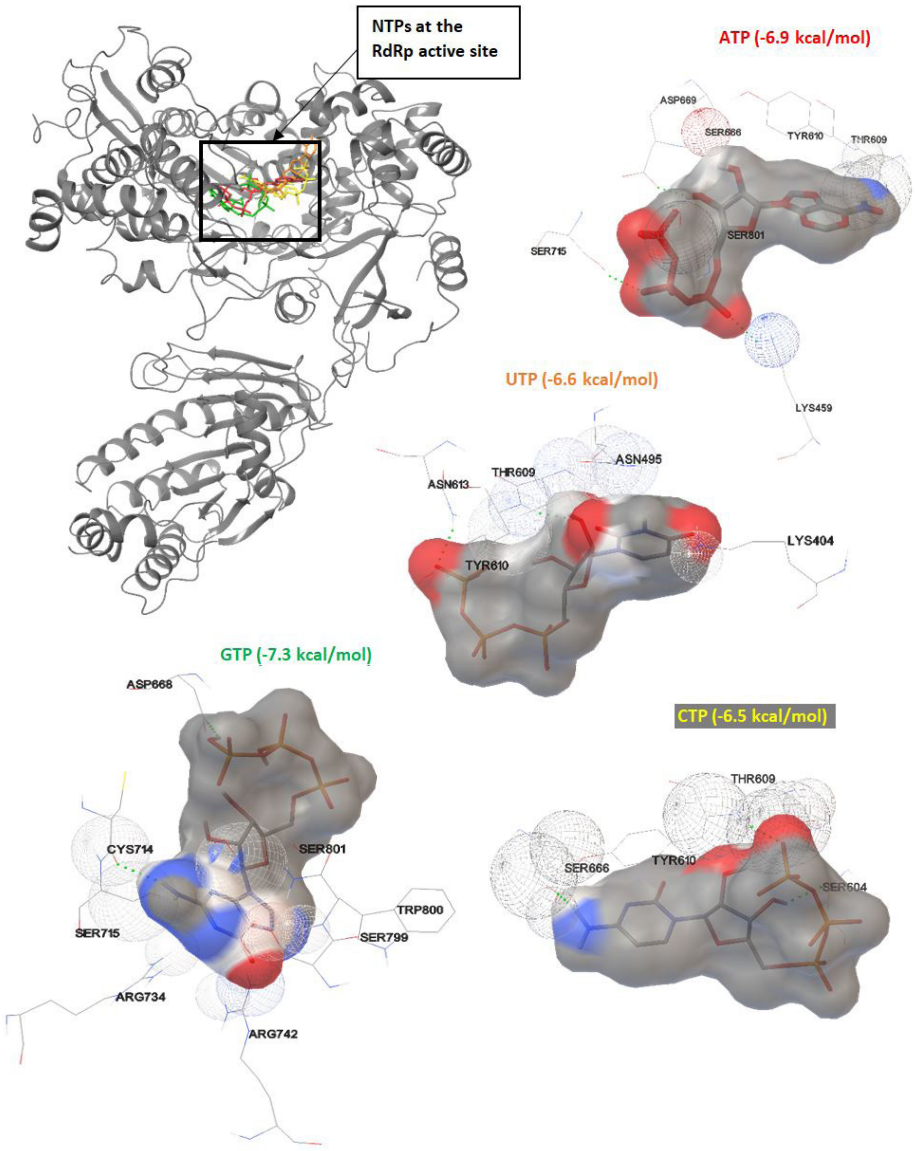

Figure 1: Interactions of NTPs with JEV NS5 at the RdRp active site. Only docking poses with the highest docking scores are shown for the representation of each ligand

Druggability Assessment of JEV NS5 protein

MD simulations of biological targets in the presence of drug-like probe molecules help characterize the ability of a target protein to bind small molecule drugs with high affinity, also known as protein druggability. The druggability of JEV NS5 protein was assessed via NAMD simulations. Figure 2 shows the system setup and analysis of the NAMD simulations. Small organic molecular probes were used to reveal any druggable sites on the receptor. After equilibration, the system was found to contain 16800 water molecules and 504 probe molecules (i.e., 306 isopropanol, 84 isobutene, 84 acetamide, 84 acetate, and 84 iso-propylamine) shown in Figure 2A. The druggability analysis revealed 330 probe binding hotspots ranging from a minimum ΔG of -2.67 kcal/mol and a maximum of -1.00 kcal/mol (Table S1). The protein surface was supplemented with 153 binding hotspots of isopropanol with the lowest binding free energy of -2.43 kcal/mol. However, isobutene (27 hotspots, -2.11 kcal/mol), isopropylamine (32 hotspots; -2.57 kcal/mol), acetamide (14 hotspots, -2.06 kcal/mol), and acetate (104 hotspots, -2.67 kcal/mol) supplementation were remote. The analysis predicted nine potential sites for drug attachment on the JEV NS5 protein (Table S2) by clustering a maximum of 7 and a minimum of 6 probes. One druggable site (Table S2: Site 2 - Solution 1) formed by a cluster of nine probe binding hotspots overlapped with the RdRp domain (Figure 2B) with an achievable binding affinity of -11.33 kcal/mol and highest drug-like affinity of 5.504 nM occupying an approximate volume of 434.83 $Å^3$ on the receptor.

Pharmacophore Identification

The hotspot information from the druggability simulations combined with the protein-NTP interaction analyses via molecular docking was used by ELIXIR-A to isolate pharmacophores for compound screening. The pharmacophoric features included proton donors or acceptors, aromatic rings, hydrophobic centroids, cations, and anions. Figure 3 illustrates the pharmacophore distribution on the JEV NS5 receptor. From the five probes tested isopropanol, followed by acetate and isobutene have the maximum affinity at the active site of the RdRp domain. Detailed information on the hotspot analysis is given under supplementary data (Table S1).

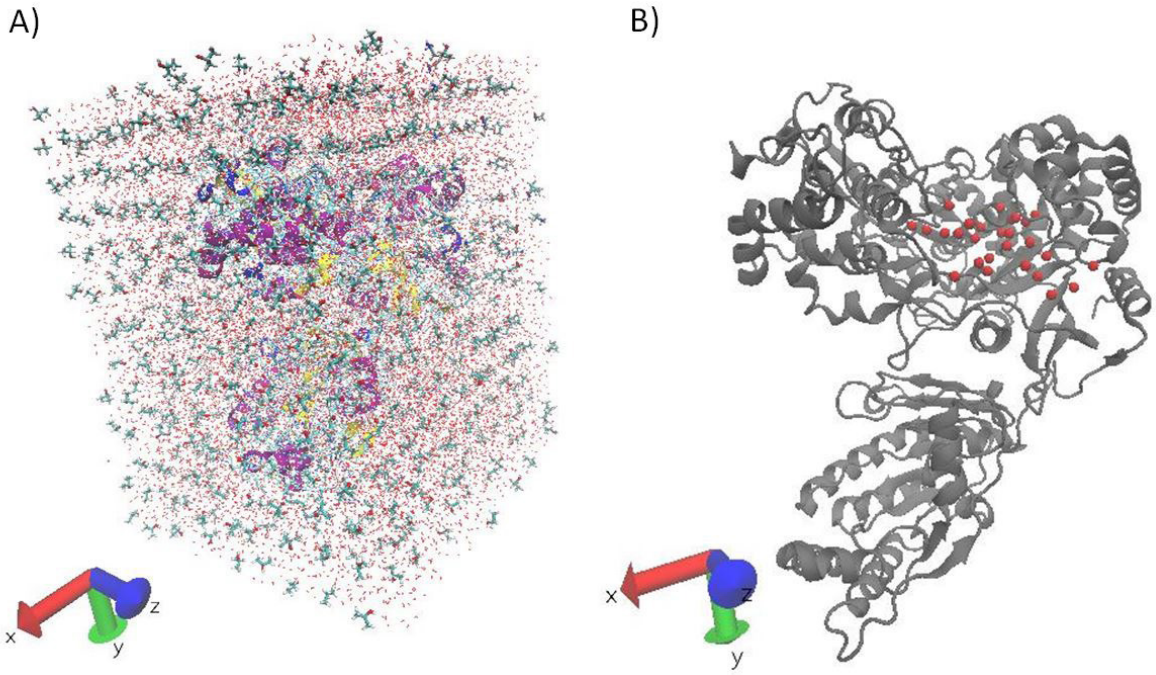

Figure 2: A) System setup for NAMD simulations. JEV NS5 protein (ribbon), water (red) and small organic probe molecules (blue licorice structures), and **B)** binding hotspots at the RdRp domain (Table S2: Site 2- Solution 1). More details on the hotspot identification process are presented under supplementary data (Table S1)

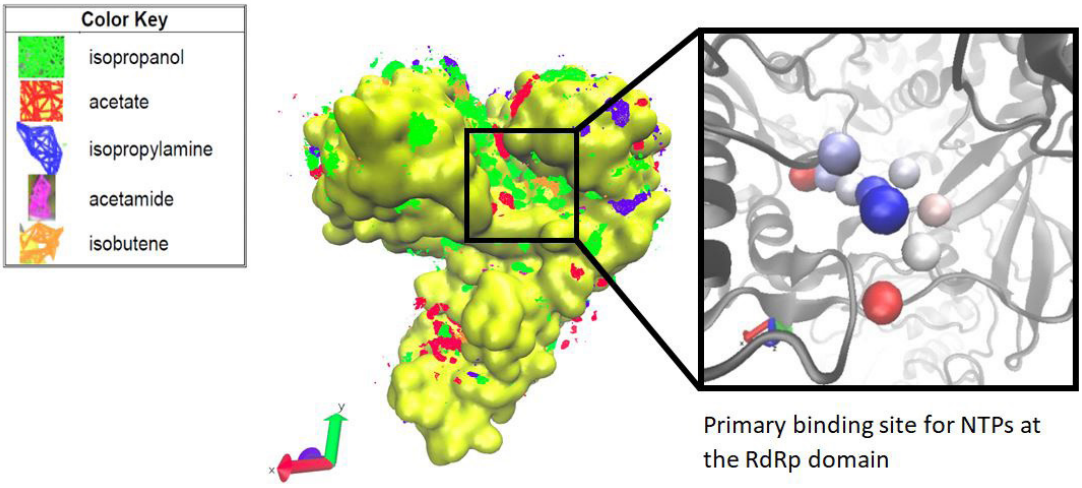

Figure 3: Hotspot (pharmacophore) distribution of JEV NS5 protein. More details on the druggability analysis are presented under supplementary data (Table S1)

Ligand Screening and Verification

With the pharmacophore information from ELIXIR-A, potential compounds were screened using the ZINCPharmer software. The screening resulted in four potential ligands: ZINC9972155, ZINC 67912950, ZINC95910070, and ZINC196939367, molecular structures of these are shown in Figure 4. Of the four identified potential drugs for JEV, ZINC 0070/chebulanin, and ZINC 9367/chebulinic acid are medicinally important phytochemicals derived from the fruit of *Terminalia*

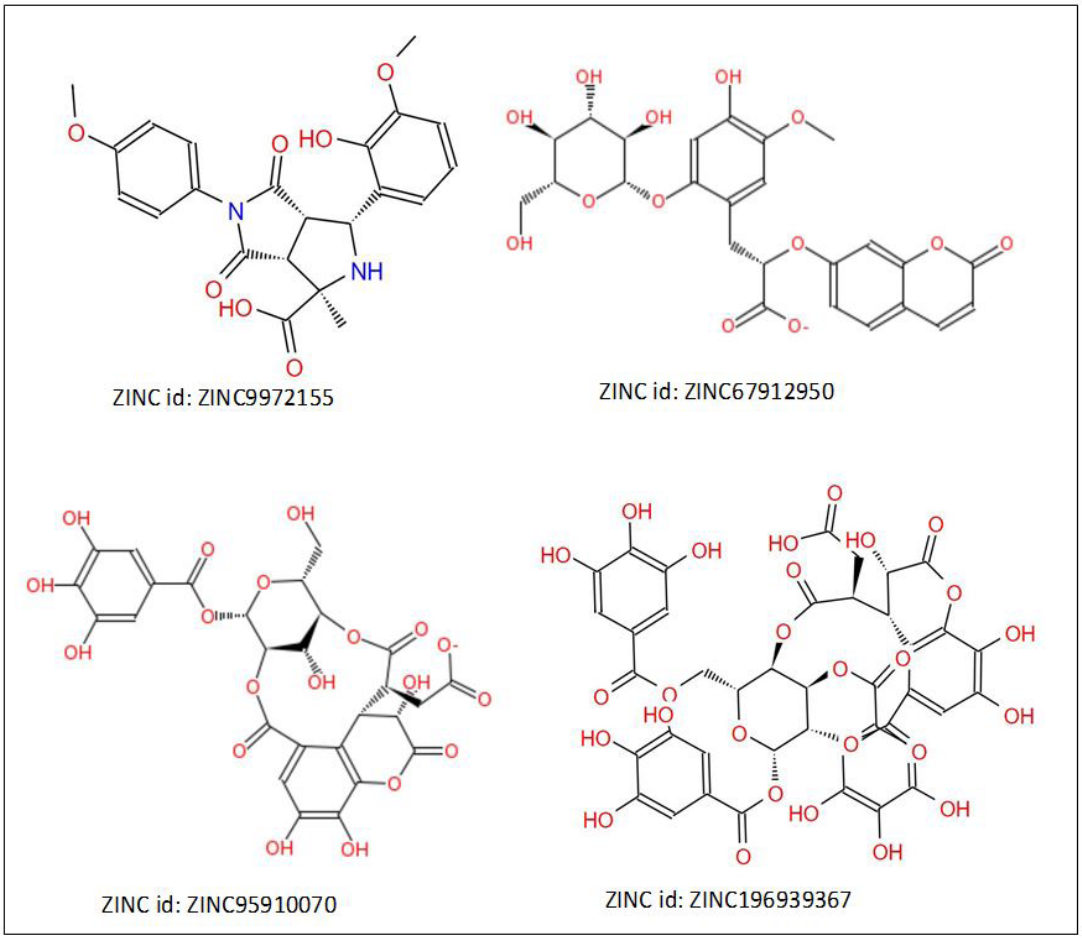

Figure 4: Potential drug molecule structures and their corresponding ZINC IDs

chebula and are active constituents of Triphala, an ancient Indian Ayurvedic medicine [41, 42]. Recent studies in arthritic mouse models revealed the anti-inflammatory and anti-arthritic effects of chebulanin [43] and antiangiogenic effects of chebulinic acid [44]. Chebulinic acid has been identified as a promising anti-tumor agent in human colorectal carcinoma and acute myeloid leukemia cell lines due to its potent anti-proliferative, pro-apoptotic, and anti-migratory properties [45, 46]. Also, chebulinic acid has been recognized for its potent direct antiviral activity against HSV-2 and influenza A virus [47, 48].

The binding affinities of ZINC 2155 (-8.1 kcal/mol) and ZINC 2950 (-8 kcal/mol) were lower (i.e., with comparatively higher binding free energies) among the four compounds. ZINC 9367 showed the highest affinity, i.e., lowest binding free energy (-11.96 kcal/mol) for the JEV NS5 protein at the RdRp domain, followed by ZINC 0070 (-9.13 kcal/mol) (Figure 5A). Clearly, ZINC 9367 and ZINC 0070 bind with a greater affinity, thus being the more promising of the four studied inhibitors. All four compounds bind at the active site of the RdRp domain where the NTP native molecules attach, as shown in Figure 5B. ZINC 9367 was able to bind into the active pocket of JEV NS5 with an affinity much higher than any of the NTPs, thus showing a high possibility of inhibiting the replication of JEV via competitive inhibition. We also compared the conformations of ATP and ZINC 9367 from our docking studies to the conformation of ATP bound at the JEV NS5 RdRp active site (PDB ID: 4HDH). The superposition of the two structures (RdRp domain from 4K6M and 4HDH) revealed an RMSD of 6.5540 Å indicative of a structural change at the RdRp domain upon ATP binding. The ligand RMSDs for docked ATP and ZINC 9367 were 4.1093 Å and 11.9828 Å respectively compared to the reference ATP from the 4HDH structure (Figure S1). ZINC 9367 binds to the native structure of RdRp in JEV with a higher affinity than the native substrates, thus capable of impeding substrate availability required for the viral replication process. Further, MD simulations were performed to verify the binding stability of ZINC 9367 into the NTP binding pocket of the RdRp domain of the JEV NS5 protein.

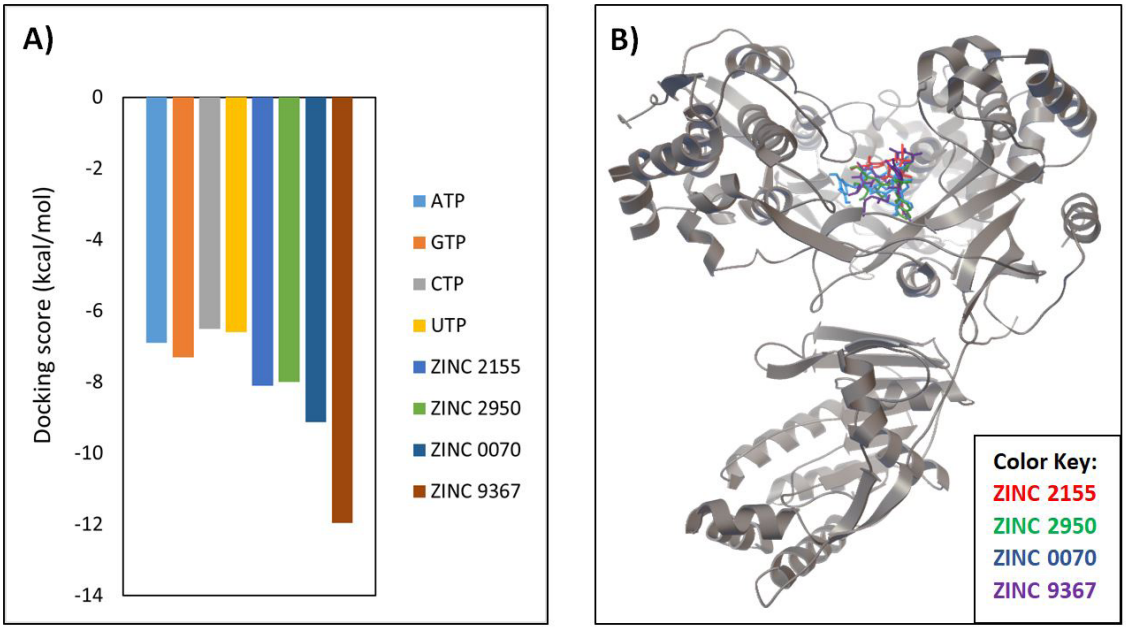

Figure 5: A) Binding affinities of all the NTPs, and screened compounds; **B)** Superimposition of docked poses of the screened compounds at the RdRp domain

MD simulations

All-atom MD simulations using explicit solvent models were employed to evaluate the stability of the JEV NS5 protein and ligand-protein complexes. The RMSD of the Cα backbone of the JEV NS5 protein complexed with ATP and ZINC 9367 are shown in Figure 6 which reveals that the ZINC 9367 complex is highly stable when compared to the native ligand ATP. The RMSD values for the protein (without ligand) were around 2.5 Å throughout the simulation. The protein backbone deviations for both the complexes were found around 3 Å over the trajectory of the simulation. Towards the end of the simulation, the ZINC 9367 complex converges to a lower RMSD value compared to the apo structure and NS5 complexed with ATP. The inset in Figure 6 illustrates the initial frame (0 ns) and the last frame (100 ns) of the whole simulation. This indicates the interaction stability of both complexes throughout the simulation.

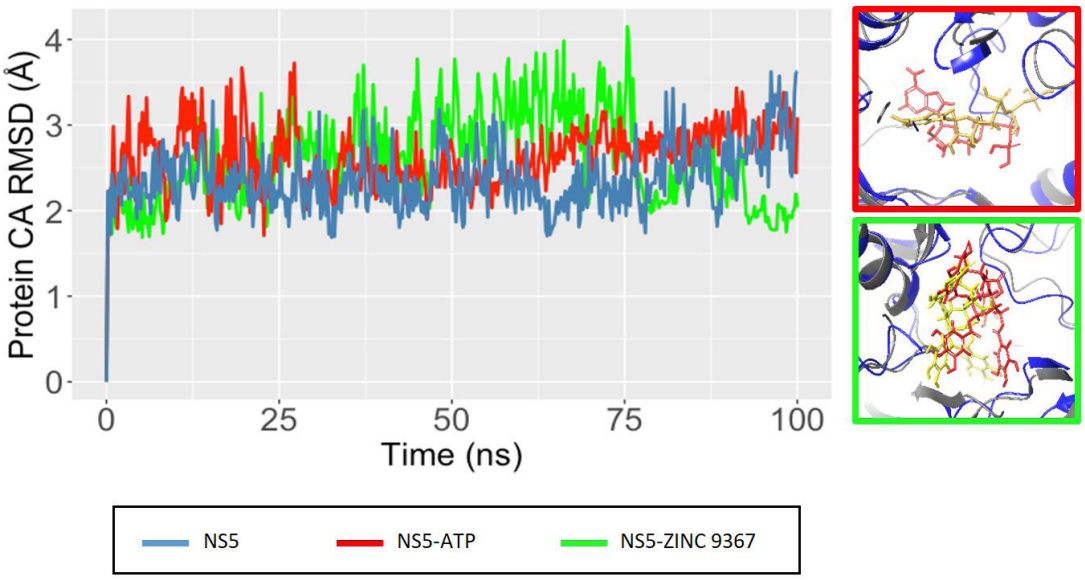

Figure 6: Protein backbone RMSD plot of JEV NS5 protein apo-structure (blue), NS5 complexed with ATP (red), and ZINC 9367 (green). Inset: The initial frame (yellow: ligand, blue: protein) and end frame (red: ligand, grey: protein) of JEV NS5 complexed with ATP (red box) and ZINC 9367 (green box) in a 100 ns simulation

The RMSF plot shown in Figure 7 supports the RMSD results. It shows that major fluctuations were observed towards the tails and in the loop regions of the protein which is typical [49,50]. The residues 255 to 280 of the NS5-ATP complex fluctuate more compared to the apo structure and NS5-ZINC 9367 complex which is due to the presence of a loop (Figure S2). Also, the NS5 protein (without ligand) and complexed with ATP show larger fluctuations around residues 850 which are towards the C-terminal of the protein compared to the NS5-ZINC 9367 complex.

The protein-ligand interaction analysis was done to explore the significant type of interactions and key protein residues involved in ligand binding for both the complexes. Figure 8 shows the histogram and schematic of protein interactions with ATP that were monitored throughout the simulation. Figure 8A reveals that ATP has strong interactions with LYS459, mainly through hydrogen bonding, hydrophobic interactions, water bridges, and some ionic interactions. It interacts with ASP669 only via water bridges and ionic interactions, and through hy-

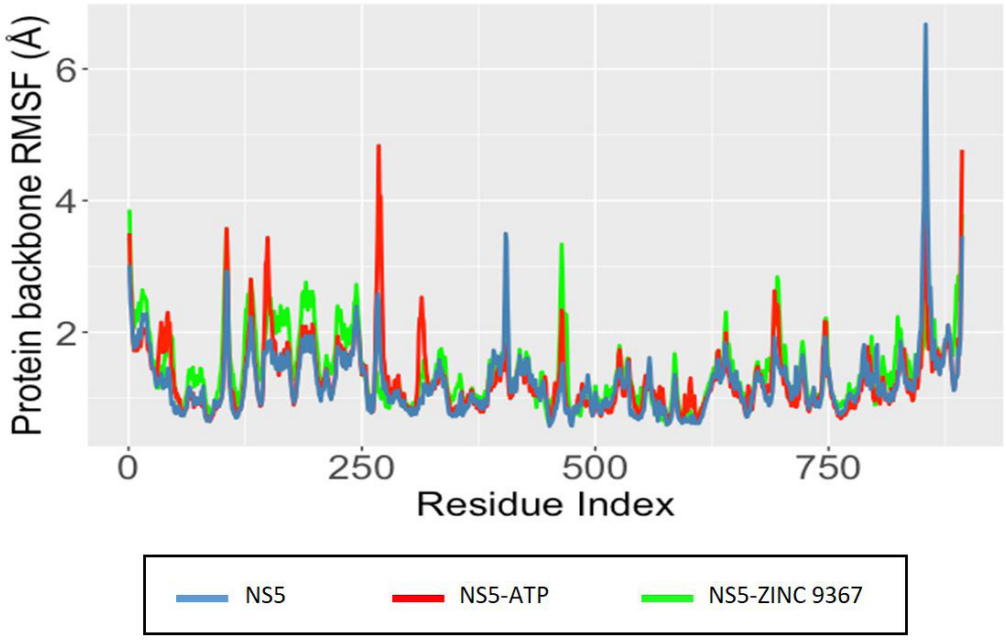

Figure 7: Protein backbone RMSF plot of JEV NS5 protein apo-structure (blue), NS5 complexed with ATP (red), and ZINC 9367 (green) over the trajectory of each system in a 100 ns simulation

drogen bonding and water bridges with SER715. These interactions of ATP with NS5 were retained from docking. While some major interactions with GLU 461, CYS 714, ARG 734, ARG 742, SER 799, TRP 800, and SER 801 were gained over a time period during the simulation.

Figure 8B shows a detailed schematic of the ATP atoms that interact with the protein residues for over 20% of the simulation time. ATP interacts with TRP 800 through hydrophobic contacts (pi-pi stacking) and hydrogen bonding. The phosphate groups of the ATP molecule form major water bridges with CYS

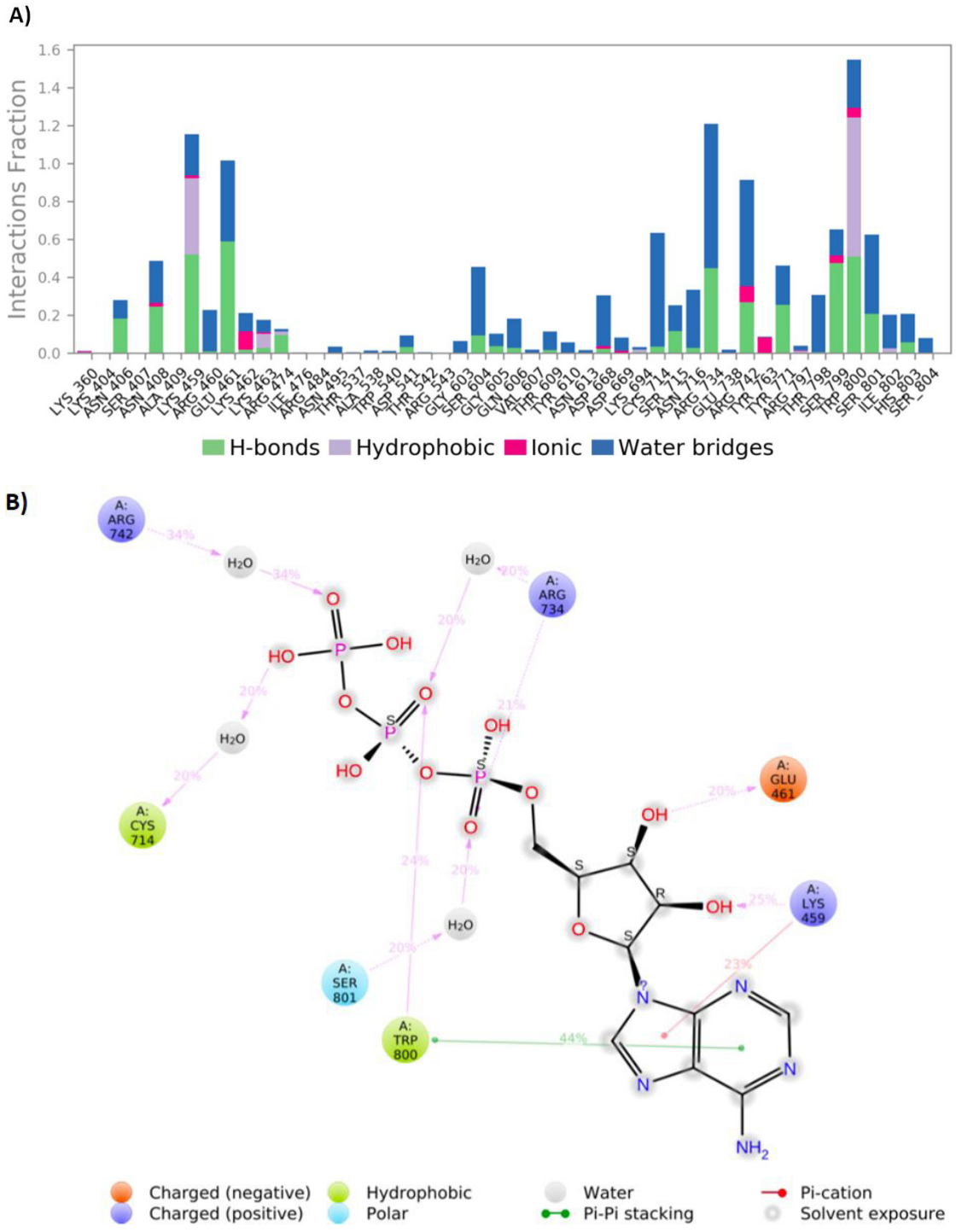

Figure 8: A) Histogram of JEV NS5-ATP interactions throughout the simulation. **B)** A schematic diagram of ATP atom interactions with the JEV NS5 protein residues. Interactions that occur more than 20.0% of the entire simulation time in the trajectory are shown

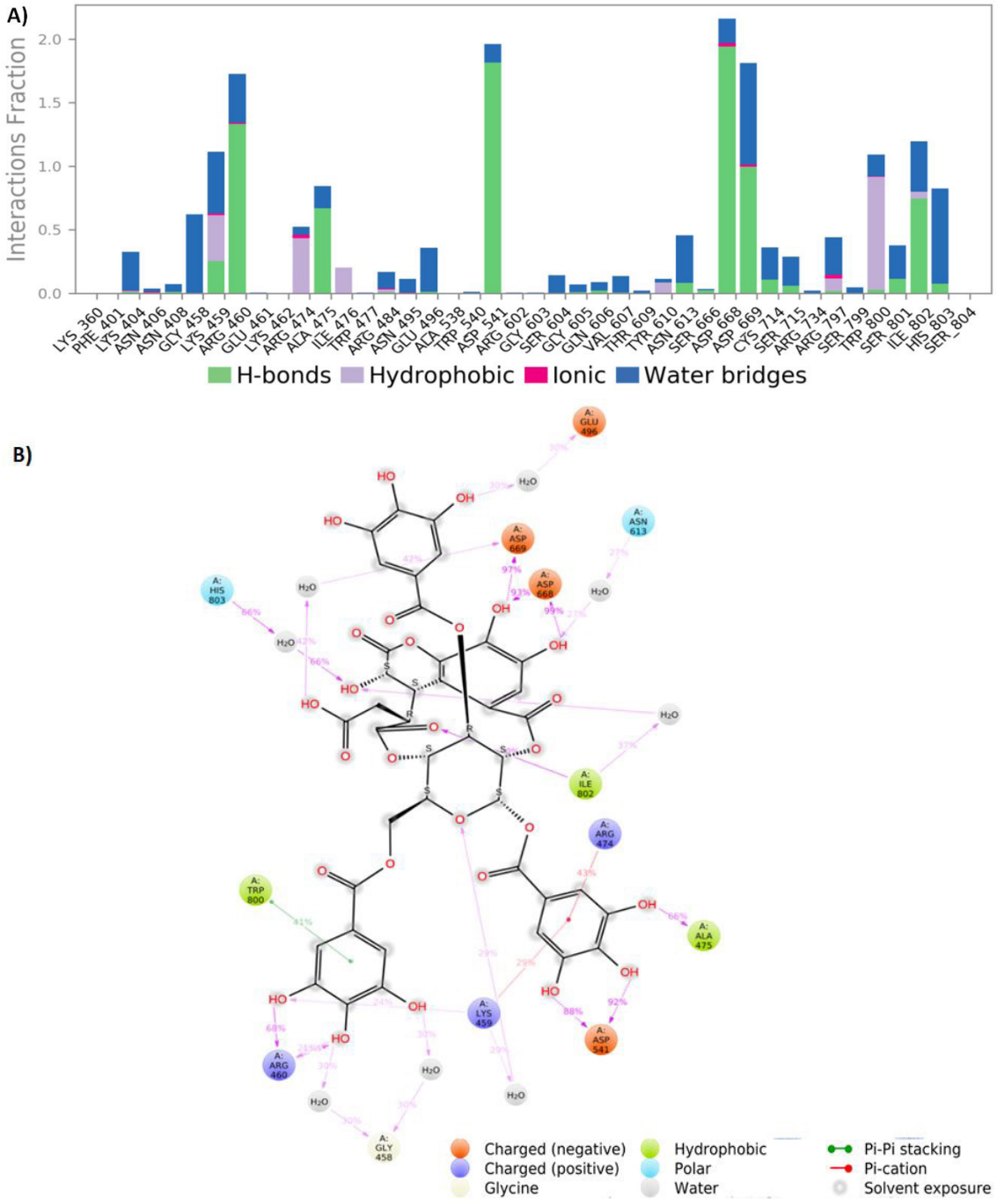

Figure 9: A) Histogram of JEV NS5-ZINC 9367 interactions throughout the simulation. **B)** A schematic diagram of ZINC 9367 atom interactions with the JEV NS5 protein residues. Interactions that occur more than 20.0% of the entire simulation time in the trajectory are shown

714, ARG 734, ARG 742, and SER 801. The ribose structure contributes to hydrogen bonding with GLU 461 and LYS 459. The aromatic rings of adenine are involved in hydrophobic contacts (pi-pi stacking) with TRP 800 for 44% of the simulation time and pi-cation interaction with LYS 459 for about 23% of the simulation time. Figure 9 gives the protein-ligand interactions for the JEV NS5- ZINC 9367 complex. It shows that ZINC-9367 forms strong interactions with LYS 459, ARG 460, ASP 541, ASP 668, ASP 669, TRP 800, ILE 802, and HIS 803. The stacked bar charts are normalized throughout the trajectory, indicating the percentage of the simulation time a specific contact is maintained. The interaction fraction values in the histograms in Figures 8A and 9A are over 1.0, which is because some protein residues are involved in multiple interactions of the same subtype with the ligands. Comparing the two histograms, clearly, ZINC 9367 is involved in a greater number of contacts with the JEV NS5 protein than ATP, which is the native ligand. Figure 9B shows that the atoms of ZINC 9367 that interact with the JEV NS5 protein residues. ZINC 9367 forms strong hydrogen bonds with ASP 541, ARG 460, ASP 668, ASP 669, and ALA 475 for more than

65% of the simulation time. Like ATP, the aromatic ring in ZINC 9367 also interacts with TRP 800 via pi-pi stacking (41%). An additional ring in ZINC 9367 is involved in pi-cation interactions with ARG 474 (43%) and LYS 459 (29%). Water-bridges are significant even in the NS5-ZINC 9367 complex.

Binding free energy calculations

Accurate prediction of receptor-ligand binding affinities is an important step in the drug discovery process. The binding free energies for protein-ligand complexes were computed using the MM/GBSA method. The distribution of MM/GBSA free energies for the two complexes over the entire trajectory during a 100 ns simulation is shown in Figure 10. The results indicate that ZINC 9367 (ΔG_{Bind} = -102.57 kcal/mol) has a higher order of binding strength compared to the native ligand ATP (ΔG_{Bind} = -43.88 kcal/mol) at the JEV NS5 RdRp active site.

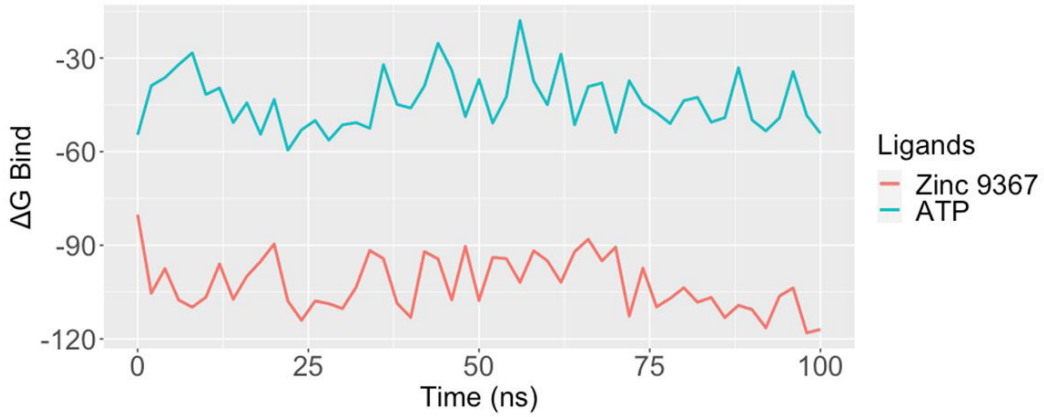

Figure 10: MM-GBSA free binding energy of ATP (blue) and ZINC 9367 (red) complexed with JEV NS5 protein. The free energy of binding (ΔGBind) is shown in kcal/mol

Conclusion

NTPs were docked on the JEV NS5 protein to determine the high binding affinity locations on the RdRp domain. Followed by a pharmacophore-based druggability analysis, four potential molecules were identified that had a high affinity to the RdRp domain. The affinities of the four lead compounds were orders of magnitude higher than that of the NTPs, the native substrates for the polymerase. Further, to decipher the binding mechanism of ZINC 9367 to the JEV NS5 receptor, a 100 ns MD simulation was performed. Protein-ligand interactions and simulation trajectory analysis revealed that ZINC 9367 forms a stable complex with JEV NS5 protein throughout the entire simulation. MM/GBSA binding free energy calculations support the docking results that ZINC 9367 has a higher binding affinity to the JEV NS5 protein than ATP. The computational results obtained in this study suggest that these compounds have a high potential to inhibit the virus by blocking RNA replication and thus are prime candidates for experimental validation via *in vitro* studies.

Data Availability

The data that support the findings of this study are available on request from the corresponding author. ELIXIR-A, the algorithm created for pharmacophore mapping has been deposited in GitHub [https://github.com/sfernando-BAEN/ELIX-IR-A].

Acknowledgment

We gratefully acknowledge the support from Texas A&M High Performance Research Computing (HPRC) and Laboratory for Molecular Simulation (LMS).

Declaration of competing interest

All the authors declare no conflict of interest.

References

1. Wang LH (2007) Japanese Encephalitis Outbreak, Yuncheng, China, 2006. Emerg Infect Diseas 13:1123-5.

2. CDC (2019) C.f.D.C.a.P. Japanese Encephalitis.

3. WHO (2019) WHO Japanese encephalitis.

4. Lindahl J (2012) Occurrence of Japanese Encephalitis Virus Mosquito Vectors in Relation to Urban Pig Holdings. The American Journal of Tropical Medicine and Hygiene 87: 1076-82.

5. Liang GX Gao, EA Gould (2015) Factors responsible for the emergence of arboviruses; strategies, challenges and limitations for their control. Emerg Microb Infect 4: e18.

6. Dash AP (2013) Emerging and re-emerging arboviral diseases in Southeast Asia. J Vector Borne Dis 50: 77-84.

7. Mackenzie JS, DJ Gubler, LR Petersen (2004) Emerging flaviviruses: the spread and resurgence of Japanese encephalitis, West Nile and dengue viruses. Nature Med10: S98.

8. Nain M (2016) Japanese encephalitis virus invasion of cell: allies and alleys. Rev Med Virol 26: 129-41.

9. Erlanger TE (2009) Past, Present, and Future of Japanese Encephalitis. Emerg Infect Diseas15: 1-7.

10. Ghosh D, A Basu (2009) Japanese Encephalitis—A Pathological and Clinical Perspective. PLOS Neglected Tropical Diseas 3: e437.

11. Fang Je (2013) Identification of Three Antiviral Inhibitors against Japanese Encephalitis Virus from Library of Pharmacologically Active Compounds 1280. PLoS ONE 8: e78425.

12. Kim JM (2008) A single N-linked glycosylation site in the Japanese encephalitis virus prM protein is critical for cell type-specific prM protein biogenesis, virus particle release, and pathogenicity in mice. J Virol 82: 7846-62.

13. Li M (2017) Japanese encephalitis virus counteracts BST2 restriction via its envelope protein E. Virol 510: 67-75.

14. Sterling T, JJ Irwin (2015) ZINC 15–ligand discovery for everyone. Journal of chemical information and modeling 55: 2324-37.

15. Lu G, P Gong (2013) Crystal Structure of the Full-Length Japanese Encephalitis Virus NS5 Reveals a Conserved Methyltransferase-Polymerase Interface. PLOS Pathogens 9: e1003549.

16. Berman HM (2000) The protein data bank. Nucleic acids res 28: 235-42.

17. Humphrey W, A Dalke, K Schulten (1996) VMD: visual molecular dynamics. J molecul graphics 14: 33-8.

18. Trott O, AJ Olson (2010) AutoDock Vina: improving the speed and accuracy of docking with a new scoring function, efficient optimization, and multithreading. Journal of computational chemistry 31: 455-61.

19. Huey R, G Morris (2003) AutoDock Tools. La Jolla, CA, USA: The Scripps Research Institute.

20. Seco J, FJ Luque, X Barril (2009) Binding Site Detection and Druggability Index from First Principles. J Med Chem 52: 2363-71.

21. Guvench O, AD MacKerell (2009) Computational Fragment-Based Binding Site Identification by Ligand Competitive Saturation. Plos Computational Biol 5.

22. Kuzmanic A (2020) Investigating Cryptic Binding Sites by Molecular Dynamics Simulations. Accounts Chem Res 53: 654-61.

23. Phillips JC (2005) Scalable molecular dynamics with NAMD. J Comput Chem 26: 1781-802.

24. Bakan A (2012) Druggability Assessment of Allosteric Proteins by Dynamics Simulations in the Presence of Probe Molecules. Journal of Chemical Theory and Computation 8: 2435-47.

25. Vanommeslaeghe K (2010) CHARMM general force field: A force field for drug-like molecules compatible with the CHARMM all-atom additive biological force fields. Journal of computational chemistry, 2010. 31(4): p. 671-690.

26. Yu W (2012) Extension of the CHARMM general force field to sulfonyl-containing compounds and its utility in biomolecular simulations. J computational chem 33: 2451-68.

27. Wang H (2019) A non-beta-lactam antibiotic inhibitor for enterohemorrhagic Escherichia coli O104: H4. J Mol Med 97: 1285-97.

28. Fernando S, T Fernando (2017) Antivirals for allosteric inhibition of Zika virus using a homology model and experimentally determined structure of envelope protein. BMC research notes 10: 1-8.

29. Gejji V (2020) An RNA-dependent RNA polymerase inhibitor for tick-borne encephalitis virus. Virology 546: 13-9.

30. Mulgaonkar N (2020) Druggability assessment of precursor membrane protein as a target for inhibiting the Zika virus. Journal of Biomolecular Structure and Dynamics, 2020: 1-17.

31. Koes DR, CJ Camacho (2012) ZINCPharmer: pharmacophore search of the ZINC database. Nucleic acids res 40: W409-W414.

32. Trott O, AJ Olson (2010) Software News and Update AutoDock Vina: Improving the Speed and Accuracy of Docking with a New Scoring Function, Efficient Optimization, and Multithreading. J Computational Chem 31: 455-61.

33. DE Shaw Research and Schrödinger L (2018) Schrödinger Release 2018-4: Desmond Molecular Dynamics System. D. E. Shaw Research, New York, NY, 2018. Maestro-Desmond Interoperability Tools, Schrödinger, New York, NY.

34. Release S4: Schrödinger Release 2018-4 Protein Preparation Wizard. New York: Schrödinger, LLC, 2018.

35. Sastry GM (2013) Protein and ligand preparation: parameters, protocols, and influence on virtual screening enrichments. Journal of computer-aided molecular design 27: 221-34.

36. Schrödinger L Schrödinger Release 2018-4: LigPrep. Schrödinger LLC: New York, NY, USA, 2018.

37. Harder E (2016) OPLS3: a force field providing broad coverage of drug-like small molecules and proteins. Journal of chemical theory and computation 12: 281-96.

38. Schrödinger L., Schrödinger Release 2018-4: Epik. Schrödinger, LLC, New York, NY, 2018., 2018.

39. Genheden S, U Ryde (2015) The MM/PBSA and MM/GBSA methods to estimate ligand-binding affinities. Expert opinion on drug discovery 10: 449-61.

40. Schrödinger, L., Schrödinger Release 2018-4: Prime. Schrödinger, LLC, New York, NY, 2020., 2018.

41. Bhatnagar S, A Rani, R Kumari (2015) Therapeutic potential of Triphala against human diseases. Int. J. Pharm. Sci. Rev. Res 31: 5-13.

42. Upadhyay A, P Agrahari, D Singh (2014) A review on the pharmacological aspects of Terminalia chebula. Int J Pharmacol 10: 289-98.

43. Liu F (2020) Chebulanin exerts its anti-inflammatory and anti-arthritic effects via inhibiting NF-κB and MAPK activation in collagen-induced arthritis mice. Int Immunopharmacol 88: 106823.

44. Lu K (2020) Chebulinic acid is a safe and effective anti-angiogenic agent in collagen-induced arthritis in mice. Arthritis research & therapy 22: 1-11.

45. Wang M, Y Li, X Hu (2018) Chebulinic acid derived from triphala is a promising antitumour agent in human colorectal carcinoma cell lines. BMC complementary and alternative med 18: 1-9.

46. Chhabra, S., et al., Chebulinic acid isolated from the fruits of Terminalia chebula specifically induces apoptosis in acute myeloid leukemia cells. Phytotherapy Res 31: 1849-1857.

47. Kesharwani A (2015) Anti-HSV-2 activity of Terminalia chebula Retz extract and its constituents, chebulagic and chebulinic acids. BMC complementary and alternative med 17: 1-11.

48. Li P (2020) Identification of Chebulinic acid and Chebulagic acid as novel influenza viral neuraminidase inhibitors. Frontiers in microbiol 11: 182.

49. Raghav PK, YK Verma, GU Gangenahalli (2012) Molecular dynamics simulations of the Bcl-2 protein to predict the structure of its unordered flexible loop domain. Journal of molecular modeling 18: 1885-1906.

50. Raghav PK, YK Verma, GU Gangenahalli (2012) Peptide screening to knockdown Bcl-2's anti-apoptotic activity: Implications in cancer treatment. International journal of biological macromolecules 50: 796-814.

Supplementary Data

Table S1: Hotspot analysis of JEV NS5

Parameter: temperature 300.00 K
Parameter: delta_g -1.000 kcal/mol
Parameter: n_probes 7
Parameter: min_n_probes 6
Parameter: merge_radius 5.5 A
Parameter: low_affinity 10.00 uM
Parameter: n_solutions 3
Parameter: max_charge 2.0 e
Parameter: n_charged 3
Parameter: n_frames 1
probe binding hotspots with deltaG less than -1.00 kcal/mol (~5 folds enrichment).
330 all-probes binding spots were identified in 3.89s.
Minimum binding free energy is -2.67 kcal/mol.
Hotspot 1 -2.67 kcal/mol 100.0% ACET
Hotspot 2 -2.57 kcal/mol 99.9% IPAM 0.1% IPRO
Hotspot 3 -2.45 kcal/mol 100.0% ACET
Hotspot 4 -2.43 kcal/mol 99.5% IPRO 0.5% ACAM
Hotspot 5 -2.37 kcal/mol 100.0% ACET
Hotspot 6 -2.34 kcal/mol 99.6% ACET 0.4% ACAM 0.0% IPAM
Hotspot 7 -2.29 kcal/mol 100.0% IPRO
Hotspot 8 -2.27 kcal/mol 99.3% ACET 0.7% IPRO
Hotspot 9 -2.24 kcal/mol 99.3% IPRO 0.7% IBUT
Hotspot 10 -2.22 kcal/mol 97.2% IPAM 2.8% IPRO
Hotspot 11 -2.16 kcal/mol 99.8% IPRO 0.2% ACET
Hotspot 12 -2.16 kcal/mol 99.5% ACET 0.5% IPRO
Hotspot 13 -2.15 kcal/mol 97.5% IPRO 2.5% IBUT
Hotspot 14 -2.13 kcal/mol 97.7% ACET 1.3% ACAM 1.1% IPRO
Hotspot 15 -2.12 kcal/mol 100.0% IPRO
Hotspot 16 -2.11 kcal/mol 61.8% IBUT 28.7% IPRO 9.5% ACAM
Hotspot 17 -2.10 kcal/mol 81.6% IPRO 18.4% ACAM
Hotspot 18 -2.09 kcal/mol 99.5% ACET 0.5% ACAM
Hotspot 19 -2.08 kcal/mol 98.9% ACET 1.1% IPRO
Hotspot 20 -2.07 kcal/mol 72.5% IPRO 26.3% IBUT 1.2% IPAM 0.1% ACAM
Hotspot 21 -2.06 kcal/mol 94.8% ACAM 5.2% IPRO
Hotspot 22 -2.06 kcal/mol 61.6% IBUT 38.4% IPRO
Hotspot 23 -2.04 kcal/mol 99.7% IPRO 0.3% IBUT
Hotspot 24 -2.03 kcal/mol 99.1% ACET 0.8% IPRO 0.1% ACAM
Hotspot 25 -1.99 kcal/mol 99.6% ACET 0.3% IPRO 0.1% ACAM
Hotspot 26 -1.97 kcal/mol 100.0% ACET
Hotspot 27 -1.96 kcal/mol 100.0% IPAM
Hotspot 28 -1.95 kcal/mol 62.9% IPRO 35.9% IBUT 1.2% ACAM
Hotspot 29 -1.92 kcal/mol 81.8% IPRO 18.2% IPAM
Hotspot 30 -1.90 kcal/mol 94.9% ACET 4.5% ACAM 0.5% IPRO
Hotspot 31 -1.90 kcal/mol 97.6% ACET 2.4% IPRO
Hotspot 32 -1.89 kcal/mol 100.0% ACET
Hotspot 33 -1.88 kcal/mol 82.4% IPRO 17.6% ACAM
Hotspot 34 -1.87 kcal/mol 75.5% IPRO 24.5% ACET
Hotspot 35 -1.87 kcal/mol 99.5% ACET 0.5% ACAM 0.1% IPRO
Hotspot 36 -1.86 kcal/mol 65.6% IBUT 21.9% ACAM 12.5% IPRO
Hotspot 37 -1.86 kcal/mol 91.5% IPRO 3.8% ACET 3.1% IPAM 1.6% ACAM
Hotspot 38 -1.86 kcal/mol 99.7% IPRO 0.3% IBUT
Hotspot 39 -1.86 kcal/mol 99.8% IPRO 0.2% IBUT
Hotspot 40 -1.85 kcal/mol 98.7% ACET 1.3% IPRO
Hotspot 41 -1.83 kcal/mol 65.3% IPRO 32.5% IBUT 2.2% ACAM
Hotspot 42 -1.83 kcal/mol 49.5% IPRO 26.8% IPAM 23.6% ACET
Hotspot 43 -1.83 kcal/mol 67.0% IBUT 32.0% IPRO 0.8% ACAM 0.2% IPAM
Hotspot 44 -1.82 kcal/mol 100.0% ACET
Hotspot 45 -1.81 kcal/mol 99.8% IPRO 0.2% ACAM
Hotspot 46 -1.81 kcal/mol 100.0% IPRO
Hotspot 47 -1.79 kcal/mol 100.0% ACET
Hotspot 48 -1.79 kcal/mol 62.5% IPAM 29.1% IPRO 4.9% IBUT 2.5% ACAM 1.0% ACET
Hotspot 49 -1.78 kcal/mol 92.3% ACET 7.7% IPRO
Hotspot 50 -1.78 kcal/mol 97.3% ACET 1.3% ACAM 1.2% IPRO 0.3% IBUT
Hotspot 51 -1.76 kcal/mol 98.7% ACET 1.3% IBUT
Hotspot 52 -1.76 kcal/mol 97.5% ACET 2.5% IPRO
Hotspot 53 -1.76 kcal/mol 100.0% IPRO
Hotspot 54 -1.75 kcal/mol 95.0% ACET 4.5% IPRO 0.3% IBUT 0.2% ACAM
Hotspot 55 -1.75 kcal/mol 60.4% IPRO 38.9% IBUT 0.6% ACAM 0.1% IPAM
Hotspot 56 -1.74 kcal/mol 90.7% IPRO 6.2% IBUT 3.0%

IPAM 0.1% ACET
Hotspot 57 -1.74 kcal/mol 100.0% IPAM
Hotspot 58 -1.73 kcal/mol 99.9% ACET 0.1% IPRO
Hotspot 59 -1.72 kcal/mol 99.8% ACET 0.2% IPRO
Hotspot 60 -1.71 kcal/mol 99.3% ACET 0.7% IPRO
Hotspot 61 -1.71 kcal/mol 84.2% IPRO 14.3% IBUT 1.5% ACAM
Hotspot 62 -1.71 kcal/mol 96.1% ACET 3.9% IPRO
Hotspot 63 -1.71 kcal/mol 97.6% ACET 2.3% IPRO 0.1% ACAM
Hotspot 64 -1.70 kcal/mol 76.8% IPRO 22.8% IBUT 0.4% IPAM
Hotspot 65 -1.70 kcal/mol 73.0% IBUT 20.6% IPRO 4.3% ACAM 2.1% IPAM
Hotspot 66 -1.69 kcal/mol 42.6% IBUT 35.8% ACET 21.5% IPRO
Hotspot 67 -1.68 kcal/mol 99.1% ACET 0.6% IPRO 0.2% ACAM
Hotspot 68 -1.68 kcal/mol 99.8% IPAM 0.2% IPRO
Hotspot 69 -1.68 kcal/mol 88.4% IPRO 11.6% IPAM
Hotspot 70 -1.68 kcal/mol 97.9% IBUT 2.1% IPRO
Hotspot 71 -1.68 kcal/mol 100.0% IPRO
Hotspot 72 -1.67 kcal/mol 98.5% IPRO 1.5% ACAM
Hotspot 73 -1.66 kcal/mol 94.8% IPRO 5.2% IBUT
Hotspot 74 -1.66 kcal/mol 100.0% IPRO
Hotspot 75 -1.66 kcal/mol 100.0% ACAM
Hotspot 76 -1.65 kcal/mol 65.0% IBUT 33.8% IPRO 1.2% ACAM
Hotspot 77 -1.65 kcal/mol 90.3% IPRO 9.7% IBUT
Hotspot 78 -1.64 kcal/mol 83.0% IBUT 15.7% IPRO 1.2% IPAM 0.1% ACAM
Hotspot 79 -1.63 kcal/mol 93.3% ACET 3.4% IPAM 3.0% ACAM 0.4% IPRO
Hotspot 80 -1.63 kcal/mol 89.4% IPRO 10.5% ACET 0.1% ACAM
Hotspot 81 -1.63 kcal/mol 86.4% IPRO 6.9% IBUT 6.1% IPAM 0.5% ACAM
Hotspot 82 -1.62 kcal/mol 91.4% ACET 8.6% IPRO
Hotspot 83 -1.62 kcal/mol 99.0% ACET 1.0% IPRO
Hotspot 84 -1.61 kcal/mol 96.9% IPAM 3.1% IPRO
Hotspot 85 -1.61 kcal/mol 93.4% IPAM 5.2% IPRO 1.4% ACAM
Hotspot 86 -1.60 kcal/mol 98.4% IPRO 1.6% IBUT
Hotspot 87 -1.59 kcal/mol 95.2% ACET 3.0% ACAM 1.7% IPRO
Hotspot 88 -1.58 kcal/mol 87.6% ACET 12.2% IPRO 0.1% ACAM
Hotspot 89 -1.58 kcal/mol 80.9% IPRO 8.3% ACAM 6.3% IBUT 4.5% IPAM
Hotspot 90 -1.58 kcal/mol 95.0% IPRO 4.2% IBUT 0.7% ACAM
Hotspot 91 -1.57 kcal/mol 75.5% ACET 24.5% ACAM
Hotspot 92 -1.56 kcal/mol 98.8% ACET 1.1% IPRO 0.2% ACAM
Hotspot 93 -1.56 kcal/mol 100.0% IPRO
Hotspot 94 -1.56 kcal/mol 67.2% IPRO 27.6% ACET 5.1% ACAM
Hotspot 95 -1.56 kcal/mol 80.6% IPRO 11.4% ACAM 8.0% IPAM
Hotspot 96 -1.56 kcal/mol 86.4% IPRO 9.9% ACET 3.7% ACAM
Hotspot 97 -1.55 kcal/mol 94.8% IPRO 4.3% IBUT 0.9% ACAM
Hotspot 98 -1.54 kcal/mol 100.0% IPAM
Hotspot 99 -1.54 kcal/mol 68.1% IBUT 31.2% IPRO 0.8% ACAM
Hotspot 100 -1.54 kcal/mol 72.6% IPRO 25.2% IBUT 2.2% ACAM
Hotspot 101 -1.54 kcal/mol 100.0% IPRO
Hotspot 102 -1.54 kcal/mol 93.6% IPAM 5.7% IPRO 0.5% ACAM 0.3% IBUT
Hotspot 103 -1.54 kcal/mol 95.9% ACET 3.3% IPRO 0.5% IPAM 0.3% ACAM
Hotspot 104 -1.53 kcal/mol 79.2% IPRO 9.8% ACET 6.2% IPAM 4.4% ACAM 0.3% IBUT
Hotspot 105 -1.51 kcal/mol 100.0% ACET
Hotspot 106 -1.50 kcal/mol 99.0% ACET 1.0% ACAM
Hotspot 107 -1.50 kcal/mol 80.9% IPRO 13.5% IBUT 3.4% ACET 2.2% ACAM
Hotspot 108 -1.49 kcal/mol 83.7% ACAM 16.3% IPRO
Hotspot 109 -1.48 kcal/mol 93.9% ACET 5.9% IPRO 0.2% ACAM
Hotspot 110 -1.47 kcal/mol 100.0% IPRO
Hotspot 111 -1.46 kcal/mol 75.8% IBUT 22.8% IPRO 1.3% ACAM 0.2% ACET
Hotspot 112 -1.45 kcal/mol 100.0% IPRO
Hotspot 113 -1.44 kcal/mol 95.0% IPRO 5.0% IBUT
Hotspot 114 -1.44 kcal/mol 100.0% ACET
Hotspot 115 -1.44 kcal/mol 70.6% ACAM 27.4% IPRO 2.0% IBUT
Hotspot 116 -1.44 kcal/mol 92.6% IPRO 4.6% ACAM 2.8% IBUT
Hotspot 117 -1.44 kcal/mol 99.4% IPAM 0.6% ACAM
Hotspot 118 -1.43 kcal/mol 52.0% IPRO 40.7% IBUT 7.3%

ACAM
Hotspot 119 -1.43 kcal/mol 74.4% IPRO 17.3% IBUT 6.8% ACET 0.8% ACAM 0.8% IPAM
Hotspot 120 -1.43 kcal/mol 84.1% IPRO 7.6% ACAM 4.2% IBUT 4.2% ACET
Hotspot 121 -1.43 kcal/mol 100.0% ACET
Hotspot 122 -1.42 kcal/mol 100.0% IPRO
Hotspot 123 -1.42 kcal/mol 98.1% ACET 1.1% ACAM 0.8% IPRO
Hotspot 124 -1.42 kcal/mol 86.9% IBUT 7.1% IPRO 6.0% IPAM
Hotspot 125 -1.42 kcal/mol 99.6% ACAM 0.4% IPRO
Hotspot 126 -1.41 kcal/mol 67.6% IPAM 26.9% IPRO 5.4% ACAM
Hotspot 127 -1.41 kcal/mol 76.1% IPRO 20.2% IBUT 2.5% ACAM 1.2% IPAM
Hotspot 128 -1.41 kcal/mol 87.8% IPAM 10.2% IPRO 2.0% ACAM
Hotspot 129 -1.39 kcal/mol 87.6% IPRO 10.0% ACAM 2.4% IPAM
Hotspot 130 -1.39 kcal/mol 100.0% ACET
Hotspot 131 -1.39 kcal/mol 97.2% ACET 1.8% IPRO 1.0% ACAM
Hotspot 132 -1.39 kcal/mol 83.6% IBUT 16.4% IPRO
Hotspot 133 -1.38 kcal/mol 84.5% IPRO 15.5% ACAM
Hotspot 134 -1.38 kcal/mol 100.0% ACAM
Hotspot 135 -1.38 kcal/mol 54.8% IPAM 28.2% IPRO 14.0% IBUT 2.9% ACAM
Hotspot 136 -1.37 kcal/mol 92.9% IPRO 7.1% ACAM
Hotspot 137 -1.37 kcal/mol 99.8% ACET 0.2% IPRO
Hotspot 138 -1.36 kcal/mol 96.6% ACET 2.7% IPRO 0.6% IPAM
Hotspot 139 -1.36 kcal/mol 99.6% ACET 0.4% IPRO
Hotspot 140 -1.36 kcal/mol 74.9% IPRO 14.6% IBUT 5.9% ACAM 4.5% IPAM
Hotspot 141 -1.35 kcal/mol 99.6% ACET 0.4% IPRO
Hotspot 142 -1.35 kcal/mol 52.0% ACAM 37.0% IPRO 11.0% IPAM
Hotspot 143 -1.34 kcal/mol 50.1% IPRO 49.9% IBUT
Hotspot 144 -1.34 kcal/mol 83.6% IPRO 16.2% IBUT 0.2% ACET
Hotspot 145 -1.34 kcal/mol 76.1% ACET 20.6% IPRO 2.4% IBUT 0.9% ACAM
Hotspot 146 -1.34 kcal/mol 61.9% IBUT 37.8% IPRO 0.2% IPAM
Hotspot 147 -1.34 kcal/mol 59.5% ACET 25.0% IPRO 10.4% IBUT 5.1% IPAM
Hotspot 148 -1.34 kcal/mol 89.6% IPRO 5.1% IBUT 3.1% ACAM 2.2% IPAM
Hotspot 149 -1.33 kcal/mol 91.1% IPRO 8.3% ACAM 0.4% IPAM 0.2% IBUT
Hotspot 150 -1.32 kcal/mol 75.2% IPRO 13.9% IPAM 10.7% ACAM 0.2% IBUT
Hotspot 151 -1.32 kcal/mol 82.0% ACET 13.9% IPRO 4.1% IBUT
Hotspot 152 -1.32 kcal/mol 100.0% ACAM
Hotspot 153 -1.31 kcal/mol 90.6% IPAM 9.2% IPRO 0.2% ACAM
Hotspot 154 -1.31 kcal/mol 86.1% IPRO 13.9% IBUT
Hotspot 155 -1.30 kcal/mol 75.5% IPAM 19.4% IPRO 2.6% IBUT 2.6% ACET
Hotspot 156 -1.30 kcal/mol 88.1% IPRO 7.7% ACAM 3.7% IBUT 0.5% ACET
Hotspot 157 -1.30 kcal/mol 96.7% ACET 3.1% IPRO 0.2% IPAM
Hotspot 158 -1.30 kcal/mol 66.2% IBUT 33.3% IPRO 0.2% ACAM 0.2% IPAM
Hotspot 159 -1.30 kcal/mol 61.2% IBUT 38.8% IPRO
Hotspot 160 -1.29 kcal/mol 97.4% ACET 2.6% IPRO
Hotspot 161 -1.29 kcal/mol 84.1% IPRO 13.7% ACAM 2.1% IBUT
Hotspot 162 -1.29 kcal/mol 100.0% IPRO
Hotspot 163 -1.29 kcal/mol 74.4% IPRO 22.2% IBUT 1.9% ACAM 1.4% IPAM
Hotspot 164 -1.28 kcal/mol 78.7% IPRO 13.3% IBUT 6.5% ACAM 1.4% IPAM
Hotspot 165 -1.28 kcal/mol 91.0% IPAM 7.8% ACAM 1.2% IPRO
Hotspot 166 -1.28 kcal/mol 91.2% IPRO 7.1% ACAM 1.7% IPAM
Hotspot 167 -1.28 kcal/mol 79.2% ACET 15.4% IPRO 4.2% IBUT 1.2% ACAM
Hotspot 168 -1.27 kcal/mol 91.9% IPAM 7.8% IPRO 0.2% ACAM
Hotspot 169 -1.27 kcal/mol 93.6% IPRO 5.9% ACAM 0.5% ACET
Hotspot 170 -1.27 kcal/mol 77.1% IPRO 11.9% ACET 6.2% IBUT 4.7% ACAM
Hotspot 171 -1.27 kcal/mol 99.5% IPAM 0.5% IPRO
Hotspot 172 -1.26 kcal/mol 67.3% IPRO 29.2% ACET 3.5% ACAM
Hotspot 173 -1.26 kcal/mol 80.8% ACET 9.2% IBUT 8.5% IPRO 1.5% ACAM
Hotspot 174 -1.26 kcal/mol 99.8% ACET 0.2% IPRO

Hotspot 175 -1.26 kcal/mol 99.5% ACET 0.5% IPRO
Hotspot 176 -1.25 kcal/mol 80.4% IPRO 17.3% IBUT 1.3% ACET 1.0% ACAM
Hotspot 177 -1.25 kcal/mol 100.0% ACET
Hotspot 178 -1.25 kcal/mol 71.2% IPRO 28.2% IPAM 0.5% ACAM
Hotspot 179 -1.25 kcal/mol 55.9% IBUT 40.3% IPRO 3.8% ACAM
Hotspot 180 -1.25 kcal/mol 81.7% ACET 18.0% IPRO 0.3% ACAM
Hotspot 181 -1.25 kcal/mol 92.5% IPRO 7.5% ACET
Hotspot 182 -1.25 kcal/mol 95.9% IPRO 4.1% ACAM
Hotspot 183 -1.25 kcal/mol 95.4% IPRO 3.6% IBUT 1.0% ACAM
Hotspot 184 -1.24 kcal/mol 91.8% ACET 8.2% IPRO
Hotspot 185 -1.24 kcal/mol 47.9% IPRO 32.7% ACET 18.3% IBUT 0.8% ACAM 0.3% IPAM
Hotspot 186 -1.24 kcal/mol 97.9% ACET 2.1% IPRO
Hotspot 187 -1.24 kcal/mol 86.2% IPRO 9.1% ACAM 4.7% IBUT
Hotspot 188 -1.24 kcal/mol 49.9% IBUT 49.1% IPRO 1.0% ACAM
Hotspot 189 -1.24 kcal/mol 100.0% IPRO
Hotspot 190 -1.24 kcal/mol 100.0% IBUT
Hotspot 191 -1.23 kcal/mol 94.8% ACET 3.7% IPRO 0.8% IPAM 0.8% IBUT
Hotspot 192 -1.23 kcal/mol 96.3% IPAM 3.7% ACET
Hotspot 193 -1.23 kcal/mol 99.7% ACET 0.3% IBUT
Hotspot 194 -1.23 kcal/mol 70.4% IPRO 19.8% ACAM 5.5% ACET 3.4% IPAM 0.8% IBUT
Hotspot 195 -1.23 kcal/mol 60.2% IPRO 36.6% IBUT 3.2% ACAM
Hotspot 196 -1.23 kcal/mol 66.0% IPRO 34.0% ACET
Hotspot 197 -1.22 kcal/mol 85.9% IPRO 14.1% IBUT
Hotspot 198 -1.22 kcal/mol 66.3% ACAM 32.3% ACET 1.3% IPRO
Hotspot 199 -1.22 kcal/mol 87.8% IPRO 11.6% IBUT 0.5% ACAM
Hotspot 200 -1.21 kcal/mol 100.0% IPRO
Hotspot 201 -1.21 kcal/mol 95.9% IPRO 4.1% ACAM
Hotspot 202 -1.21 kcal/mol 49.9% IPRO 47.7% IBUT 2.2% IPAM 0.3% ACAM
Hotspot 203 -1.21 kcal/mol 100.0% ACET
Hotspot 204 -1.20 kcal/mol 78.5% IPRO 21.5% IBUT
Hotspot 205 -1.20 kcal/mol 93.9% IPRO 3.6% ACAM 1.9% IPAM 0.3% ACET 0.3% IBUT
Hotspot 206 -1.20 kcal/mol 68.4% IPRO 19.4% ACAM 12.2% IBUT
Hotspot 207 -1.20 kcal/mol 99.4% ACAM 0.6% IPRO
Hotspot 208 -1.20 kcal/mol 100.0% ACET
Hotspot 209 -1.19 kcal/mol 72.8% IPRO 25.8% IBUT 1.1% ACAM 0.3% IPAM
Hotspot 210 -1.19 kcal/mol 64.8% IPRO 24.5% IBUT 6.2% ACAM 4.5% ACET
Hotspot 211 -1.18 kcal/mol 51.0% IBUT 47.6% IPRO 1.4% ACAM
Hotspot 212 -1.18 kcal/mol 90.3% ACAM 9.7% IPRO
Hotspot 213 -1.18 kcal/mol 71.2% ACET 28.8% IPRO
Hotspot 214 -1.18 kcal/mol 99.4% ACET 0.6% IPRO
Hotspot 215 -1.18 kcal/mol 54.9% IPAM 45.1% IPRO
Hotspot 216 -1.17 kcal/mol 63.2% IPRO 33.9% IBUT 2.9% ACAM
Hotspot 217 -1.17 kcal/mol 58.0% IPRO 23.5% IBUT 14.2% ACAM 4.3% IPAM
Hotspot 218 -1.17 kcal/mol 79.4% ACAM 20.0% IPRO 0.6% IBUT
Hotspot 219 -1.17 kcal/mol 100.0% IPAM
Hotspot 220 -1.17 kcal/mol 100.0% IPAM
Hotspot 221 -1.17 kcal/mol 83.7% IPRO 15.4% IBUT 0.9% ACAM
Hotspot 222 -1.17 kcal/mol 79.9% IPRO 12.5% IBUT 7.6% IPAM
Hotspot 223 -1.17 kcal/mol 99.1% IPAM 0.6% IPRO 0.3% ACAM
Hotspot 224 -1.17 kcal/mol 59.6% IBUT 40.1% IPRO 0.3% ACAM
Hotspot 225 -1.17 kcal/mol 57.3% IPRO 36.0% ACAM 6.7% IBUT
Hotspot 226 -1.17 kcal/mol 76.8% IBUT 23.2% IPRO
Hotspot 227 -1.17 kcal/mol 71.5% IPRO 15.9% IBUT 11.5% ACET 1.2% ACAM
Hotspot 228 -1.16 kcal/mol 77.0% IPRO 16.2% IBUT 4.7% ACAM 2.1% IPAM
Hotspot 229 -1.16 kcal/mol 94.7% ACET 2.4% IPRO 1.5% ACAM 1.2% IBUT 0.3% IPAM
Hotspot 230 -1.16 kcal/mol 62.5% IPRO 29.8% IBUT 4.8% IPAM 3.0% ACAM
Hotspot 231 -1.15 kcal/mol 98.8% ACET 0.6% ACAM 0.6% IPRO
Hotspot 232 -1.15 kcal/mol 85.0% ACET 14.7% IPRO 0.3% ACAM
Hotspot 233 -1.15 kcal/mol 57.1% IPRO 22.8% IPAM 16.5% ACAM 2.7% IBUT 0.9% ACET
Hotspot 234 -1.15 kcal/mol 99.7% ACET 0.3% IPRO

Hotspot 235 -1.15 kcal/mol 97.3% ACET 2.7% IPRO
Hotspot 236 -1.15 kcal/mol 90.3% IPRO 8.8% ACAM 0.9% ACET
Hotspot 237 -1.15 kcal/mol 100.0% IPRO
Hotspot 238 -1.14 kcal/mol 37.2% IBUT 32.3% IPRO 30.5% IPAM
Hotspot 239 -1.14 kcal/mol 98.8% ACET 0.9% IPRO 0.3% ACAM
Hotspot 240 -1.14 kcal/mol 89.3% IPRO 6.1% IBUT 4.6% ACAM
Hotspot 241 -1.14 kcal/mol 100.0% IPRO
Hotspot 242 -1.14 kcal/mol 82.5% IPRO 6.8% ACET 5.8% IBUT 4.0% IPAM 0.9% ACAM
Hotspot 243 -1.14 kcal/mol 98.8% ACET 0.9% IPRO 0.3% ACAM
Hotspot 244 -1.13 kcal/mol 98.1% ACET 1.6% IPRO 0.3% ACAM
Hotspot 245 -1.13 kcal/mol 56.2% ACET 36.6% IPRO 3.8% ACAM 3.4% IBUT
Hotspot 246 -1.13 kcal/mol 52.4% IPRO 23.8% IPAM 16.9% ACAM 6.9% ACET
Hotspot 247 -1.12 kcal/mol 98.1% ACET 0.6% ACAM 0.6% IPAM 0.6% IPRO
Hotspot 248 -1.12 kcal/mol 98.4% ACET 0.9% IBUT 0.6% IPRO
Hotspot 249 -1.12 kcal/mol 93.1% IPRO 6.9% IBUT
Hotspot 250 -1.12 kcal/mol 100.0% ACAM
Hotspot 251 -1.11 kcal/mol 98.4% IPRO 1.6% ACAM
Hotspot 252 -1.11 kcal/mol 98.7% IPRO 1.3% IBUT
Hotspot 253 -1.11 kcal/mol 78.8% IPRO 11.3% ACAM 10.0% IPAM
Hotspot 254 -1.10 kcal/mol 56.0% ACET 24.8% IPRO 19.2% IPAM
Hotspot 255 -1.10 kcal/mol 81.3% IPRO 13.4% ACAM 5.2% IPAM
Hotspot 256 -1.10 kcal/mol 70.5% ACET 29.5% IPRO
Hotspot 257 -1.10 kcal/mol 94.1% IPRO 3.9% IBUT 2.0% IPAM
Hotspot 258 -1.10 kcal/mol 100.0% ACET
Hotspot 259 -1.10 kcal/mol 80.5% IPRO 19.1% ACAM 0.3% IBUT
Hotspot 260 -1.10 kcal/mol 53.6% IPRO 34.8% ACET 11.6% ACAM
Hotspot 261 -1.10 kcal/mol 65.9% IPAM 29.8% IPRO 3.0% ACAM 1.3% IBUT
Hotspot 262 -1.09 kcal/mol 50.8% IPRO 31.2% IPAM 17.9% ACAM
Hotspot 263 -1.09 kcal/mol 78.3% ACET 21.7% IPRO
Hotspot 264 -1.09 kcal/mol 44.7% IBUT 40.3% IPRO 13.3% ACAM 1.3% ACET 0.3% IPAM
Hotspot 265 -1.09 kcal/mol 97.3% IPAM 2.7% IPRO
Hotspot 266 -1.09 kcal/mol 96.0% IPRO 2.7% IBUT 1.3% ACAM
Hotspot 267 -1.09 kcal/mol 84.2% IPRO 7.7% ACAM 7.0% IPAM 1.0% ACET
Hotspot 268 -1.09 kcal/mol 67.1% ACET 31.9% IPRO 1.0% ACAM
Hotspot 269 -1.09 kcal/mol 48.0% IBUT 28.5% IPRO 12.4% IPAM 10.7% ACAM 0.3% ACET
Hotspot 270 -1.09 kcal/mol 59.1% IPRO 35.2% IBUT 4.4% IPAM 1.3% ACAM
Hotspot 271 -1.09 kcal/mol 80.8% IPRO 19.2% IBUT
Hotspot 272 -1.08 kcal/mol 84.8% IPRO 10.1% IPAM 2.0% IBUT 1.7% ACAM 1.4% ACET
Hotspot 273 -1.08 kcal/mol 89.9% ACET 9.5% IPRO 0.7% ACAM
Hotspot 274 -1.08 kcal/mol 39.2% IPAM 31.1% ACAM 29.1% IPRO 0.7% ACET
Hotspot 275 -1.08 kcal/mol 67.8% IPRO 31.9% IBUT 0.3% ACAM
Hotspot 276 -1.08 kcal/mol 59.5% IPRO 40.5% IPAM
Hotspot 277 -1.08 kcal/mol 95.2% IPRO 3.1% ACAM 1.7% IPAM
Hotspot 278 -1.08 kcal/mol 56.5% ACET 38.1% IPRO 4.8% IBUT 0.7% ACAM
Hotspot 279 -1.08 kcal/mol 99.3% IPRO 0.7% ACET
Hotspot 280 -1.08 kcal/mol 73.5% IPRO 16.7% IPAM 7.8% ACAM 2.0% ACET
Hotspot 281 -1.08 kcal/mol 74.1% IPRO 25.9% IBUT
Hotspot 282 -1.08 kcal/mol 98.3% IPRO 1.4% ACAM 0.3% ACET
Hotspot 283 -1.08 kcal/mol 95.9% ACET 2.7% IPRO 0.7% ACAM 0.7% IPAM
Hotspot 284 -1.08 kcal/mol 68.2% IPRO 31.5% IBUT 0.3% ACAM
Hotspot 285 -1.08 kcal/mol 44.2% IPRO 39.4% IBUT 16.1% IPAM 0.3% ACAM
Hotspot 286 -1.07 kcal/mol 86.9% IPAM 11.3% IPRO 1.7% ACAM
Hotspot 287 -1.07 kcal/mol 100.0% IPRO
Hotspot 288 -1.07 kcal/mol 73.2% IPRO 18.9% IBUT 4.8% ACAM 3.1% ACET
Hotspot 289 -1.07 kcal/mol 83.8% IPRO 10.7% IBUT 5.5% ACAM

Hotspot 290 -1.07 kcal/mol 100.0% ACAM
Hotspot 291 -1.06 kcal/mol 77.7% IPRO 19.9% ACAM 1.7% IBUT 0.7% ACET
Hotspot 292 -1.06 kcal/mol 93.3% IPRO 6.4% IPAM 0.4% ACAM
Hotspot 293 -1.05 kcal/mol 61.7% IPRO 37.9% IBUT 0.4% ACAM
Hotspot 294 -1.05 kcal/mol 95.7% IPRO 2.8% IBUT 1.4% ACAM
Hotspot 295 -1.05 kcal/mol 98.2% IPAM 1.1% ACAM 0.4% ACET 0.4% IPRO
Hotspot 296 -1.05 kcal/mol 100.0% IPRO
Hotspot 297 -1.05 kcal/mol 99.3% ACET 0.7% IPRO
Hotspot 298 -1.05 kcal/mol 86.4% ACET 8.6% IPRO 2.9% ACAM 2.1% IBUT
Hotspot 299 -1.05 kcal/mol 83.6% ACET 12.1% IPRO 2.1% IPAM 1.4% IBUT 0.7% ACAM
Hotspot 300 -1.05 kcal/mol 100.0% ACET
Hotspot 301 -1.05 kcal/mol 84.3% IPRO 11.1% IBUT 4.3% ACAM 0.4% ACET
Hotspot 302 -1.05 kcal/mol 100.0% ACET
Hotspot 303 -1.05 kcal/mol 98.6% IPAM 1.4% IPRO
Hotspot 304 -1.05 kcal/mol 98.2% ACET 1.8% IPRO
Hotspot 305 -1.05 kcal/mol 86.4% ACET 9.7% IPAM 3.6% ACAM 0.4% IPRO
Hotspot 306 -1.04 kcal/mol 99.3% IPRO 0.7% IBUT
Hotspot 307 -1.04 kcal/mol 97.1% IPAM 2.6% ACAM 0.4% IPRO
Hotspot 308 -1.04 kcal/mol 100.0% IPRO
Hotspot 309 -1.04 kcal/mol 98.9% ACET 0.7% IBUT 0.4% IPRO
Hotspot 310 -1.04 kcal/mol 99.6% IPAM 0.4% ACAM
Hotspot 311 -1.03 kcal/mol 65.1% IPRO 21.0% IBUT 14.0% ACAM
Hotspot 312 -1.03 kcal/mol 68.3% IPRO 15.5% ACAM 11.4% IBUT 4.8% IPAM
Hotspot 313 -1.03 kcal/mol 51.1% IPRO 33.7% IBUT 15.2% ACAM
Hotspot 314 -1.02 kcal/mol 77.9% ACET 15.4% IPRO 6.4% IPAM 0.4% ACAM
Hotspot 315 -1.02 kcal/mol 96.3% IPRO 3.4% ACAM 0.4% ACET
Hotspot 316 -1.02 kcal/mol 79.2% IPRO 13.6% IPAM 6.8% IBUT 0.4% ACAM
Hotspot 317 -1.01 kcal/mol 61.5% IPRO 36.3% IBUT 2.3% ACAM
Hotspot 318 -1.01 kcal/mol 79.3% IPRO 11.1% ACAM 7.7% IBUT 1.9% IPAM
Hotspot 319 -1.01 kcal/mol 92.3% IPRO 5.7% ACAM 1.9% IBUT
Hotspot 320 -1.01 kcal/mol 48.7% ACET 37.5% IPRO 13.8% ACAM
Hotspot 321 -1.01 kcal/mol 84.6% IPRO 15.4% ACAM
Hotspot 322 -1.01 kcal/mol 91.9% ACET 8.1% IPRO
Hotspot 323 -1.01 kcal/mol 70.8% IPRO 16.2% IBUT 13.1% ACET
Hotspot 324 -1.01 kcal/mol 96.5% ACET 2.7% IPRO 0.8% ACAM
Hotspot 325 -1.00 kcal/mol 96.5% ACET 3.5% IPRO
Hotspot 326 -1.00 kcal/mol 95.4% ACET 1.9% ACAM 1.5% IPRO 1.2% IPAM
Hotspot 327 -1.00 kcal/mol 97.3% ACET 2.3% IPRO 0.4% IPAM
Hotspot 328 -1.00 kcal/mol 56.8% IBUT 35.9% IPRO 6.9% ACAM 0.4% ACET
Hotspot 329 -1.00 kcal/mol 67.1% IBUT 30.2% IPRO 2.7% ACAM
Hotspot 330 -1.00 kcal/mol 53.9% ACET 40.3% IPRO 5.8% IBUT
IPRO: 153 isopropanol binding hotspots were identified.
IPRO: lowest binding free energy is -2.43 kcal/mol.
IBUT: 27 isobutane binding hotspots were identified.
IBUT: lowest binding free energy is -2.11 kcal/mol.
IPAM: 32 isopropylamine binding hotspots were identified.
IPAM: lowest binding free energy is -2.57 kcal/mol.
ACAM: 14 acetamide binding hotspots were identified.
ACAM: lowest binding free energy is -2.06 kcal/mol.
ACET: 104 acetate binding hotspots were identified.
ACET: lowest binding free energy is -2.67 kcal/mol.
Clustering probe binding hotspots.
Clustering completed in 1.74ms.

Table S2: Druggability analysis of JEV NS5

9 potential sites are identified.
Calculating achievable affinity ranges.
Site 1: 27 probe binding hotspots
Site 1: Lowest probe binding free energy -2.67 kcal/mol
Site 1: Average probe binding free energy-1.52 kcal/mol
Site 1: Total of 259 solutions.

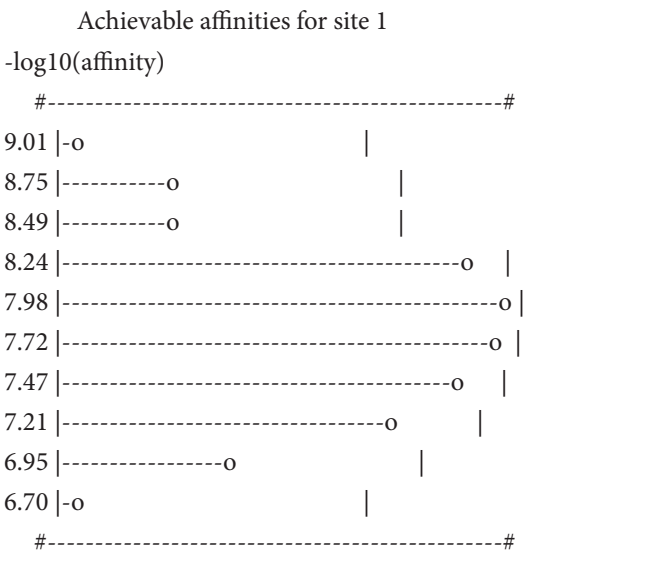

Site 1: Lowest drug-like binding free energy -12.36 kcal/mol
Site 1: Highest drug-like affinity 0.982 nM
Site 1: Solution 1 binding free energy -12.36 kcal/mol
Site 1: Solution 1 affinity 0.982 nM
Site 1: Solution 1 total charge -1.92 e
Site 1: Solution 1 number of hotspots 7
Site 1: Solution 1 approximate volume 428.57 A^3
Site 1: Solution 2 binding free energy -12.01 kcal/mol
Site 1: Solution 2 affinity 1.759 nM
Site 1: Solution 2 total charge -1.92 e
Site 1: Solution 2 number of hotspots 7
Site 1: Solution 2 approximate volume 431.26 A^3
Site 1: Solution 3 binding free energy -11.95 kcal/mol
Site 1: Solution 3 affinity 1.946 nM
Site 1: Solution 3 total charge -1.93 e
Site 1: Solution 3 number of hotspots 7
Site 1: Solution 3 approximate volume 447.06 A^3
Site 2: 9 probe binding hotspots
Site 2: Lowest probe binding free energy -2.15 kcal/mol
Site 2: Average probe binding free energy-1.54 kcal/mol
Site 2: Total of 18 solutions.

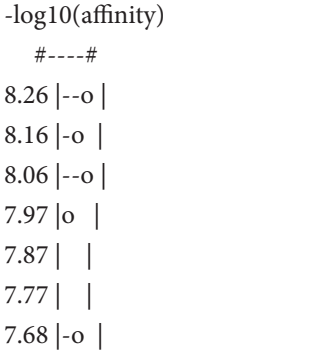

Site 2: Lowest drug-like binding free energy -11.33 kcal/mol
Site 2: Highest drug-like affinity 5.504 nM
Site 2: Solution 1 binding free energy -11.33 kcal/mol
Site 2: Solution 1 affinity 5.504 nM
Site 2: Solution 1 total charge -0.42 e
Site 2: Solution 1 number of hotspots 7
Site 2: Solution 1 approximate volume 434.83 A^3
Site 2: Solution 2 binding free energy -11.28 kcal/mol
Site 2: Solution 2 affinity 5.986 nM
Site 2: Solution 2 total charge -0.42 e
Site 2: Solution 2 number of hotspots 7
Site 2: Solution 2 approximate volume 437.02 A^3
Site 2: Solution 3 binding free energy -11.20 kcal/mol
Site 2: Solution 3 affinity 6.846 nM
Site 2: Solution 3 total charge -0.42 e
Site 2: Solution 3 number of hotspots 7
Site 2: Solution 3 approximate volume 428.28 A^3
Site 3: 10 probe binding hotspots
Site 3: Lowest probe binding free energy -2.16 kcal/mol
Site 3: Average probe binding free energy-1.49 kcal/mol
Site 3: Lowest drug-like binding free energy -11.16 kcal/mol
Site 3: Highest drug-like affinity 7.380 nM
Site 3: Solution 1 binding free energy -11.16 kcal/mol
Site 3: Solution 1 affinity 7.380 nM
Site 3: Solution 1 total charge -1.59 e
Site 3: Solution 1 number of hotspots 7
Site 3: Solution 1 approximate volume 465.81 A^3
Site 4: 19 probe binding hotspots
Site 4: Lowest probe binding free energy -2.45 kcal/mol
Site 4: Average probe binding free energy-1.48 kcal/mol
Site 4: Lowest drug-like binding free energy -10.59 kcal/mol
Site 4: Highest drug-like affinity 19.109 nM
Site 4: Solution 1 binding free energy -10.59 kcal/mol
Site 4: Solution 1 affinity 19.109 nM
Site 4: Solution 1 total charge 1.05 e
Site 4: Solution 1 number of hotspots 7
Site 4: Solution 1 approximate volume 469.24 A^3
Site 5: 11 probe binding hotspots
Site 5: Lowest probe binding free energy -2.07 kcal/mol
Site 5: Average probe binding free energy-1.32 kcal/mol
Site 5: Total of 11 solutions.

Achievable affinities for site 5

-log10(affinity)

#-----#

7.36 |---o |

7.28 |o |

7.19 | |

7.11 | |

7.02 | |

6.94 | |

6.85 |o |

6.77 |o |

6.68 |-o |

6.60 |-o |

#-----#

0

Site 5: Lowest drug-like binding free energy -10.10 kcal/mol

Site 5: Highest drug-like affinity 43.311 nM

Site 5: Solution 1 binding free energy -10.10 kcal/mol

Site 5: Solution 1 affinity 43.311 nM

Site 5: Solution 1 total charge 0.08 e

Site 5: Solution 1 number of hotspots 7

Site 5: Solution 1 approximate volume 446.84 A^3

Site 5: Solution 2 binding free energy -10.06 kcal/mol

Site 5: Solution 2 affinity 46.783 nM

Site 5: Solution 2 total charge 0.02 e

Site 5: Solution 2 number of hotspots 7

Site 5: Solution 2 approximate volume 463.89 A^3

Site 5: Solution 3 binding free energy -10.00 kcal/mol

Site 5: Solution 3 affinity 51.689 nM

Site 5: Solution 3 total charge 1.05 e

Site 5: Solution 3 number of hotspots 7

Site 5: Solution 3 approximate volume 459.74 A^3

Site 6: 6 probe binding hotspots

Site 6: Lowest probe binding free energy -1.99 kcal/mol

Site 6: Average probe binding free energy-1.59 kcal/mol

Site 6: Lowest drug-like binding free energy -9.52 kcal/mol

Site 6: Highest drug-like affinity 0.115 uM

Site 6: Solution 1 binding free energy -9.52 kcal/mol

Site 6: Solution 1 affinity 0.115 uM

Site 6: Solution 1 total charge -1.99 e

Site 6: Solution 1 number of hotspots 6

Site 6: Solution 1 approximate volume 333.92 A^3

Site 7: 13 probe binding hotspots

Site 7: Lowest probe binding free energy -1.68 kcal/mol

Site 7: Average probe binding free energy-1.21 kcal/mol

Site 7: Total of 57 solutions.

Achievable affinities for site 7 -log10(affinity)

#-----------#

6.80 |---o |

6.71 |---------o |

6.63 |------o |

6.55 |---o |

6.47 |-----o |

6.39 |---------o |

6.30 |---------o |

6.22 |--o |

6.14 | |

6.06 |--o |

#-----------#

0 5 10

Site 7: Lowest drug-like binding free energy -9.32 kcal/mol

Site 7: Highest drug-like affinity 0.160 uM

Site 7: Solution 1 binding free energy -9.32 kcal/mol

Site 7: Solution 1 affinity 0.160 uM

Site 7: Solution 1 total charge 0.00 e

Site 7: Solution 1 number of hotspots 7

Site 7: Solution 1 approximate volume 460.21 A^3

Site 7: Solution 2 binding free energy -9.31 kcal/mol

Site 7: Solution 2 affinity 0.162 uM

Site 7: Solution 2 total charge 0.00 e

Site 7: Solution 2 number of hotspots 7

Site 7: Solution 2 approximate volume 450.33 A^3

Site 7: Solution 3 binding free energy -9.27 kcal/mol

Site 7: Solution 3 affinity 0.175 uM

Site 7: Solution 3 total charge 0.00 e

Site 7: Solution 3 number of hotspots 7

Site 7: Solution 3 approximate volume 439.12 A^3

Site 8: 6 probe binding hotspots

Site 8: Lowest probe binding free energy -2.12 kcal/mol

Site 8: Average probe binding free energy-1.55 kcal/mol

Site 8: Lowest drug-like binding free energy -9.29 kcal/mol

Site 8: Highest drug-like affinity 0.170 uM

Site 8: Solution 1 binding free energy -9.29 kcal/mol

Site 8: Solution 1 affinity 0.170 uM

Site 8: Solution 1 total charge 1.21 e

Site 8: Solution 1 number of hotspots 6

Site 8: Solution 1 approximate volume 360.82 A^3

Site 9: 7 probe binding hotspots

Site 9: Lowest probe binding free energy -1.67 kcal/mol

Site 9: Average probe binding free energy-1.29 kcal/mol

Site 9: Lowest drug-like binding free energy -9.04 kcal/mol

Site 9: Highest drug-like affinity 0.256 uM

Site 9: Solution 1 binding free energy -9.04 kcal/mol
Site 9: Solution 1 affinity 0.256 uM
Site 9: Solution 1 total charge 0.00 e
Site 9: Solution 1 number of hotspots 7
Site 9: Solution 1 approximate volume 391.65

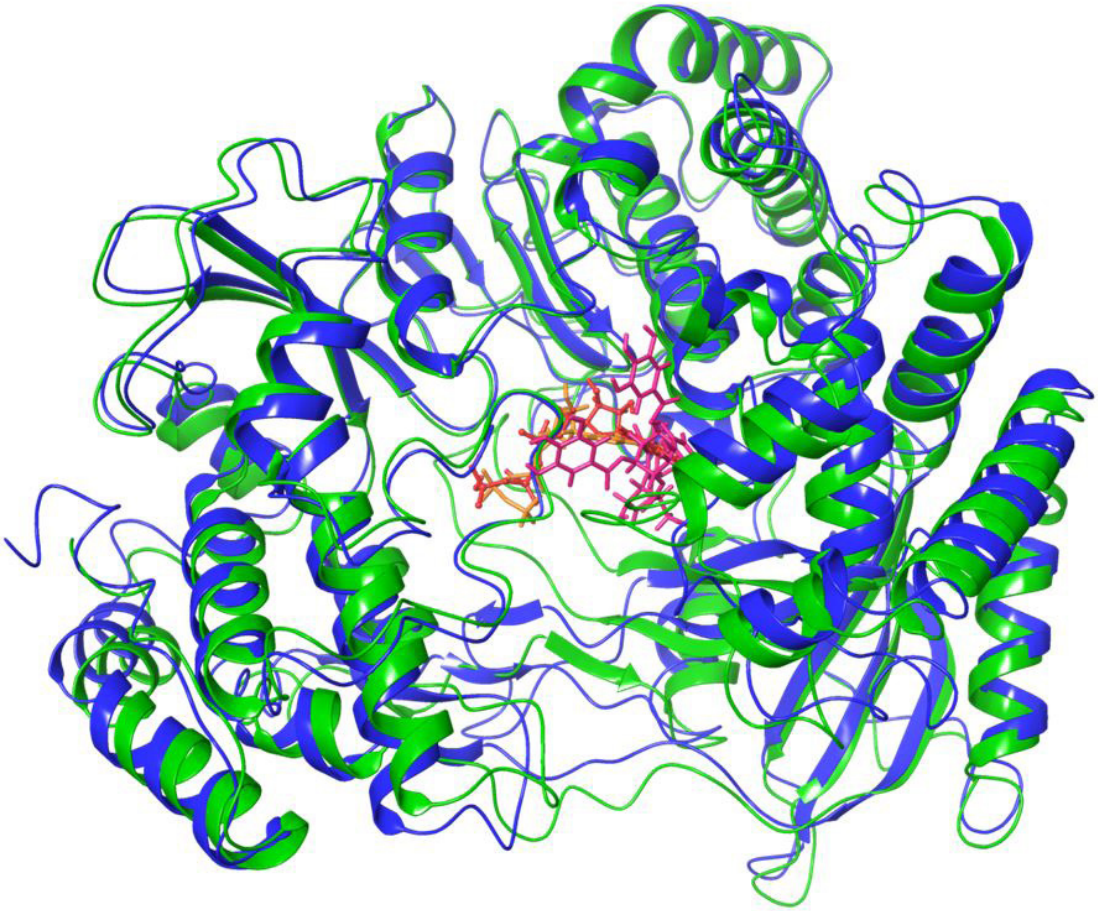

Figure S1: Structural superposition of JEV NS5 RdRp domains: 4K6M apo-structure (blue) and ATP-bound crystal structure 4HDH (green). The RMSD for 4HDH relative to the 4K6M structure is 6.5540 Å. The original substrate ATP (4HDH) is shown in orange. The RMSD for docked ATP (red) and ZINC 9367 (purple) was 4.1093 Å and 11.9828 Å respectively compared to the reference original substrate ATP

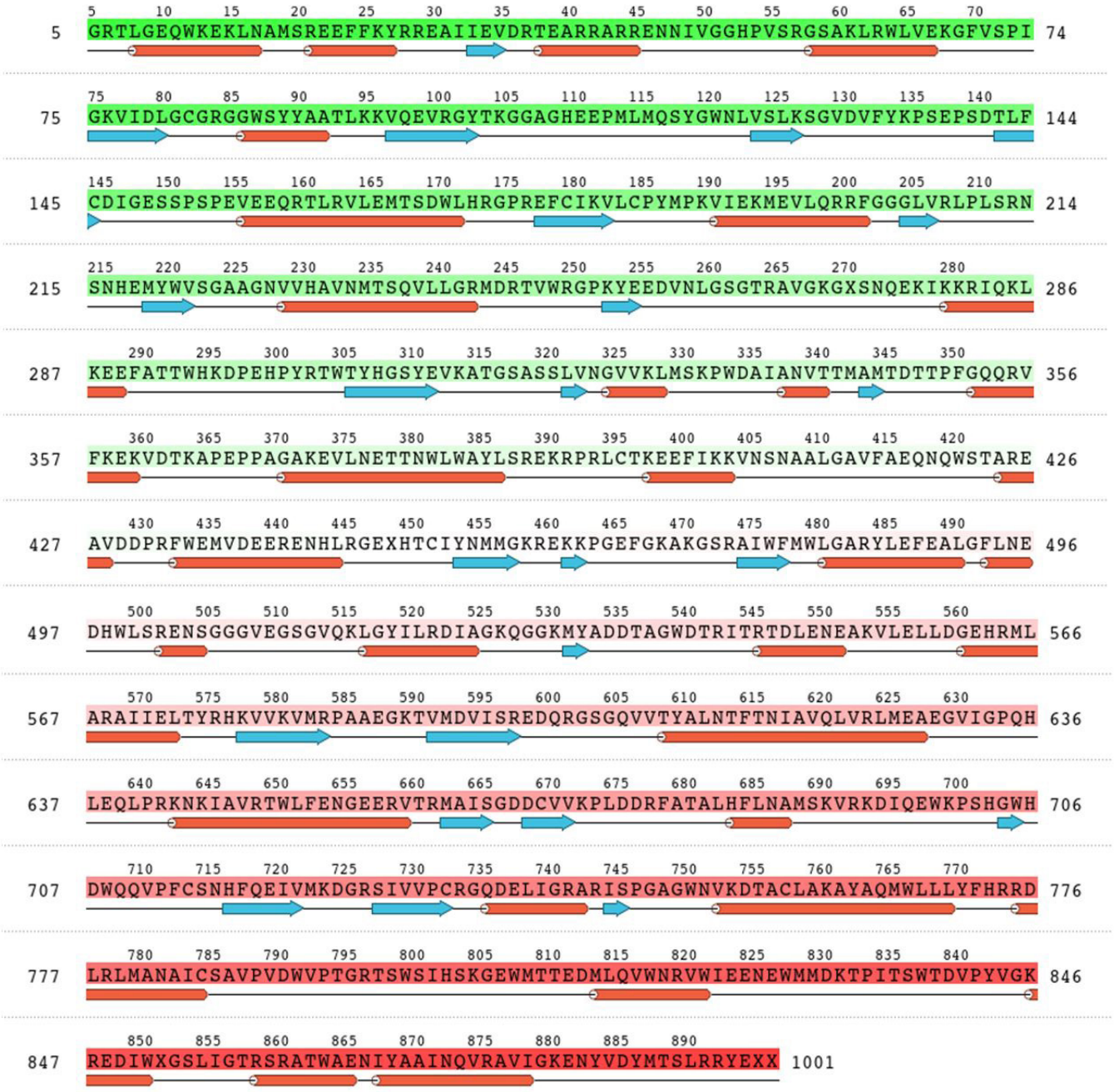

Figure S2: JEV NS5 protein (PDB: 4K6M chain A) information. Total number of residues = 893. Alpha-helical (red cylinders) and beta-strand (blue arrows) regions connected by loops (black lines) are shown